TECHNICAL NOTE

D - 775

AERODYNAMIC CHARACTERISTICS OF A LARGE-SCALE MODEL WITH A HIGH DISK-LOADING LIFTING FAN MOUNTED IN THE FUSELAGE

By Kiyoshi Aoyagi, David H. Hickey,
and Richard A. deSavigny

Ames Research Center
Moffett Field, Calif.

NATIONAL AERONAUTICS AND SPACE ADMINISTRATION

WASHINGTON

October 1961

NATIONAL AERONAUTICS AND SPACE ADMINISTRATION

TECHNICAL NOTE D-775

AERODYNAMIC CHARACTERISTICS OF A LARGE-SCALE MODEL WITH A HIGH DISK-LOADING LIFTING FAN MOUNTED IN THE FUSELAGE

By Kiyoshi Aoyagi, David H. Hickey,
and Richard A. deSavigny

SUMMARY

An investigation was conducted to determine the longitudinal characteristics during low-speed flight of a large-scale VTOL airplane model with a direct lifting fan enclosed in the fuselage. The model had a shoulder-mounted unswept wing of aspect ratio 5. The effects on longitudinal characteristics of fan operation, propulsion by means of deflecting the fan efflux, trailing-edge flap deflection, and horizontal-tail height were studied.

The lifting-fan performance characteristics, three-component longitudinal characteristics, static-pressure distributions over some parts of the model, and downwash at the horizontal tail are included herein.

INTRODUCTION

Small-scale studies of direct lifting fans mounted in a wing, reported in references 1, 2, and 3, indicated the feasibility of this V/STOL concept. The low disk loading of the fans employed and the low Reynolds number of these investigations made results questionable when applied to aircraft designs with high disk-loading fans. With the advent of the General Electric X-353-5 lifting-fan engine, it became possible to make an investigation with full-scale disk loadings and Reynolds numbers over the complete low-speed, fan-supported portion of the flight envelope.

The configuration selected for this investigation had the fan and duct mounted in the fuselage to provide a good flow environment for the fan, and a shoulder-mounted wing to minimize ground effect. The fan was mounted at the wing quarter chord and was fitted with duct exit vanes to vector the fan flow for propulsion. The wing was fitted with full-span single-slotted flaps to provide more flexibility in low-speed flight. Longitudinal control was supplied by a variable-incidence horizontal tail and a jet reaction control located at the tail.

Engine inlet performance, general aerodynamic characteristics, and longitudinal stability and control characteristics were obtained. Limited data at a predetermined lift, with drag and moment trimmed out, were obtained over a speed range from 0 to 100 knots.

These results are presented without discussion to expedite publication. A limited analysis of some of the results is presented in reference 4.

NOTATION

A	fan exit area, sq ft
b	wing span, ft
c	wing chord parallel to plane of symmetry or vane chord, ft
c_e	fan exit vane chord, ft
c_f	flap chord parallel to plane of symmetry, ft
$\bar{c}$	mean aerodynamic chord, $\frac{2}{S}\int_0^{b/2} c^2 dy$
C_F	fan thrust coefficient, $\frac{\text{thrust on fan rotor}}{q_\infty S}$
C_L	lift coefficient, $\frac{L}{q_\infty S}$
C_D	drag coefficient, $\frac{D}{q_\infty S}$
C_m	pitching-moment coefficient, $\frac{M}{q_\infty S\bar{c}}$
ΔC_m	pitching-moment increment
D	drag, lb
HP	gas horsepower
i_t	horizontal-tail incidence angle, deg
L	total lift on model, lb
M	moment about wing $0.25\bar{c}$, ft/lb
p_l	local static pressure, lb/sq ft

p_s test section static pressure, lb/sq ft

P pressure coefficient, $\frac{p_l - p_s}{q_\infty}$

P_o pressure at standard atmosphere, 2116 lb/sq ft

P_t total pressure, lb/sq ft

q dynamic pressure, lb/sq ft

R Reynolds number or fan radius, ft

RPM corrected fan rotational speed

r distance from fan rotational axis, in.

S wing area, sq ft

T complete ducted fan thrust in the lift direction, $\rho A v_j^2$, lb

v air velocity, ft/sec

V air velocity, knots

W fan weight rate of flow, lb/sec

x distance from leading edge of the airfoil flap, or of the vane, ft

y spanwise distance perpendicular to the plane of symmetry, ft

z perpendicular distance from the chord line to the airfoil flap, or vane surface, ft

α angle of attack of fuselage reference line, deg

β fan exit vane deflection measured normal to the pivot line and from the fan axis, deg

δ relative static pressure, $\frac{p_s}{p_o}$

δ_f trailing-edge flap deflection measured normal to the hinge line, deg

ϵ average downwash angle at the horizontal tail, deg

η fraction of wing semispan, $\frac{2y}{b}$

η_f spanwise extent of the trailing-edge flap, fraction of semispan

θ ratio of absolute ambient temperature to standard temperature, 519° R

μ tip-speed ratio, $\frac{V_{\infty}}{\omega R}$

ρ density, lb sec^2/ft^4

ω rotational speed, radians/sec

Subscripts

c fan rotor face

f fan

j fan exit

r reaction control

s static condition

v forward speed condition

x variable

w wing

∞ free stream

β variable exit vane angle

MODEL AND APPARATUS

Photographs of the model mounted in the Ames 40- by 80-Foot Wind Tunnel are presented in figure 1. A sketch of the model giving pertinent dimensions is shown in figure 2.

Wing Geometry

The wing had an aspect ratio of 5.0, taper ratio of 0.5, and sweepback of 0° at the quarter-chord line. The wing upper surface was tangent with the top of the fuselage. NACA 63A-210 sections parallel to the model symmetrical center line were employed. Coordinates of the wing section are listed in table I.

Details of the single-slotted trailing-edge flap are shown in figure 3, and flap ordinates are shown in table II. The flap extended over the full span of the wing, with a chordwise break at 60-percent semispan, so that short or full-span flaps could be tested. Flap deflections of 0°, 15°, 30°, and 40° were tested.

Fuselage

A sketch of the fuselage is shown in figure 4. The front portion of the fuselage had an elliptical plan view with a 3.67- by 11.42-foot semiaxis and an elliptical side view with a 2.83- by 11.42-foot semiaxis. Cross sections were also elliptical. The middle portion which housed the fan unit had a constant, essentially rectangular cross section. The afterportion had a straight taper from a 5.04- by 6.44-foot elliptical cross section to a 1.64- by 1.44-foot elliptical cross section.

Longitudinal Controls

Tail.- Geometry of the horizontal and vertical tails is given in figure 2. The all-movable horizontal tail pivoted about the quarter-chord line and could be mounted at either 0.2 or 0.4 of the wing semispan above the extended wing chord plane. Most of the testing was done at the 0.4 semispan height. Tail incidence could be varied from -23° to +45°. When it was desired to trim out moments at high lift, a 0.30-chord full-span split flap deflected 30° was added to the horizontal tail. The vertical tail had no movable control surface and was used mainly to mount the horizontal tail.

Pitch reaction control system.- Air for the reaction control was provided by a modified aircraft supercharger driven by two variable-speed electric motors (see fig. 4). Air flow from the reaction control nozzle could be directed either up or down by means of an actuated valve located inside the nozzle. The amount of reactive force was changed by varying the speed of the supercharger.

Lift-Fan Unit

The General Electric X-353-5 lifting-fan engine consists of a fan driven by exhaust gases from a gas generator. The fan was designed for a J-85 gas generator. A J85-3 was used for the first phase of the test program, and a J85-7 for the second phase. The exhaust gases are channeled through a turbine at the tip of the fan.

Fan details.- The fan was mounted near the bottom of the fuselage. A suspension framework supported the J-85 gas generator below and to the right of the fuselage. Details of the installation are shown in figures 2 and 5. During the second phase of the tests, the vertical section of the exhaust duct was faired with a teardrop fairing, and a stub wing fairing was placed over the protrusions on the right side of the fuselage. Data with these fairings installed are noted as being from the second phase of the investigation.

The single-stage fan rotor had 36 blades and a 62.5-inch diameter. A single stage of stators was employed behind the rotor. Exit vanes were mounted downstream of the stators. These vanes could be deflected from -15° to $+75^{\circ}$ (full duct closure). The span of the vanes extended across the tip turbine exhaust. The vane airfoil section had a maximum thickness of 10-percent chord at 20-percent chord and had a maximum of 2.3-percent-chord camber of the mean line at 35-percent chord.

Fan inlet.- A sketch of the inlet is shown in figure 5(d). The front half of the inlet (coordinates in table III) had a varying radius from 0.23 to 0.06 of the fan diameter; the rear half had a constant radius of 0.06 of the fan diameter. A semicircular inlet vane with a 22.71-inch chord was mounted in the front portion of the inlet. The vane airfoil section was made up of a 6-inch wedge attached to the trailing edge of a conventional airfoil section. The upper side of the wedge was tangent to the upper surface of the airfoil trailing edge and the lower side was faired into the bottom of the airfoil. The resultant airfoil section was 10-percent-chord thick with 10.5-percent-chord camber of the mean line.

TESTING AND PROCEDURE

Force and moment data were obtained through an angle-of-attack range from -8° to $+18^{\circ}$. Some fan performance and pressure distributions on the wing and fuselage were also measured. The airspeed of the tests varied from 0 to 100 knots, corresponding to a maximum Reynolds number of 7.9 million. Fan RPM was varied from 1200 to 2600 RPM.

Tests With Constant Angle of Attack

At 0° angle of attack, fan speed and wind-tunnel velocity were varied. The results were obtained for several exit-vane deflections, three flap deflections, two flap spans, and horizontal tail off and at two heights from the wing chord plane.

When it was desired to trim the model in drag and moment with a specified lift, an angle of attack was selected, and fan RPM, exit-vane angle, stabilizer angle, and reaction control were adjusted to give the desired result.

Tests With Varying Angle of Attack

Fan RPM was maintained essentially constant when angle of attack was varied. These data were obtained at several values of RPM and tunnel airspeed. The model variables tested in this manner are the same as those mentioned above.

CORRECTIONS

Wind-Tunnel Corrections

Force data obtained without fan operation were corrected for the effect of wind-tunnel wall interference as follows:

$$\alpha = \alpha_u + 0.533\ C_{L_u}$$

$$C_D = C_{D_u} + 0.0093\ C_{L_u}^2$$

$$C_m = C_{m_u} - 0.0194\ C_{L_u}\ \text{(Tail test only)}$$

No corrections were made to the force data obtained with fan operation since the effect of the fan air flow on wind-tunnel corrections is unknown.

Tares

Corrections due to the model support struts have not been incorporated in the test results. The drag coefficient of the support struts is estimated to be 0.02. Removal of the gas generator and vertical section of the exhaust duct from the model reduced the model drag coefficient 0.02 at $\alpha = 0^\circ$. The addition of fairings to the engine tail pipe and mounts did not change the drag coefficient.

It should be realized that the air flowing through the gas generator makes small contributions to lift, drag, and moment. The test results include these forces and moments.

RESULTS

These results cover the fan-supported flight-speed range from 0 to 100 knots. For convenience, the results are presented in two groups: fan and installation characteristics and general aerodynamic characteristics of the complete model. Results presented were obtained in two

separate wind-tunnel tests. Data from the second test are denoted on the figures. Partial fairings in the gas generator area and a more powerful gas generator (J85-7) were used in the second program.

Installed Fan Characteristics

Zero airspeed.- Figures 6 through 8 present fan characteristics near zero forward speed. Figure 6 presents lift, fan air flow, and gas horsepower versus fan RPM. The gas horsepower was measured at the inlet of the fan turbine nozzle. Lift is presented versus thrust (negative drag) for several power settings and exit-vane angle settings in figure 7. Figure 8 presents the variation of lift, drag, and moment with fan RPM for several exit-vane angle settings.

Forward speed.- Many independent parameters can be substituted for wind-tunnel dynamic pressure and fan RPM. Perhaps the most basic parameter is V_∞/V_j; however, V_j is difficult to measure. Tip-speed ratio, μ, is easily measured but has little physical significance unless the fan is the exact duplicate of a flight article. As the fan tested for this investigation is intended to be flight hardware, tip-speed ratio will be used herein. For those who would prefer to analyze the data with another parameter, figure 9 shows the relationship between C_F, V_∞/V_j, and μ for $\beta = 0^\circ$. Total-pressure measurements downstream from the fan rotor established these relationships.

Figures 10 through 13 show the fan operating characteristics. Figure 10 shows the increase in fan thrust and air flow with forward speed (tip-speed ratio). This is shown in the form of the ratio of thrust or air flow at forward speed to the value at zero forward speed for the same fan RPM. Figure 11 presents results showing the effect of exit-vane angle on fan thrust and air flow at several forward speeds. The ratio of fan thrust or air flow at some exit-vane angle to the thrust or air flow at 0° exit-vane angle is employed in the presentation. Data in both figures 10 and 11 were obtained from pressure instrumentation upstream and downstream from the fan rotor. Figure 12 shows the ram recovery of the inlet as a function of forward speed (tip-speed ratio) with and without the inlet vane installed. Figure 13 presents corresponding data showing the effect of angle of attack on the inlet ram recovery for several tip-speed ratios. Ram recovery is defined as $1 - [(P_{t_\infty} - P_{t_c})/q_\infty]$ where P_{t_c} is the average total pressure measured in front of the fan rotor.

Aerodynamic Characteristics of the Model

0° angle of attack.- Figures 14 through 19 show the effect of fan power and airspeed (tip-speed ratio) on various aerodynamic characteristics

at 0° angle of attack. Figure 14 shows the variation of the ratio of lift at some airspeed to zero airspeed lift at the same fan RPM as a function of tip-speed ratio for four trailing-edge flap configurations. Figures 15 and 16 present the variation of lift, drag, and pitching-moment coefficients with tip-speed ratio at $\alpha = 0^\circ$. Figure 15 shows the effect of trailing-edge flap configuration and figure 16 shows the effect of exit-vane angle deflection with the tail off and at two heights from the wing chord plane. Figure 17 shows pressure distributions on the top and bottom of the fuselage at four tip-speed ratios and three exit-vane deflections with $\alpha = 0^\circ$. Pressure distributions on the wing of the model were integrated to provide wing lift and moment coefficients. These data are shown in figure 18 as a function of tip-speed ratio for three exit-vane angles and $\alpha = 0^\circ$. The variation with tip-speed ratio of the average downwash at the horizontal tail, computed from the data in figure 16, is shown in figure 19 for two tail heights.

Variable angle-of-attack results.- Figures 20 through 23 present data showing longitudinal characteristics with the fan power off. Figure 20 shows the characteristics for three full-span trailing-edge flap configurations with and without the horizontal tail. Figure 21 shows the effect of partial-span flap deflection and horizontal-tail position. Figure 22 presents data with the inlet open and with the exit vanes open and closed. Figure 23 shows the effect of Reynolds number on longitudinal characteristics.

Figures 24 through 28 present the longitudinal characteristics with the lifting fan operating. The characteristics at 20 knots airspeed are presented in pounds and foot-pounds, and at higher speeds the characteristics are in airplane coefficient form. Figure 24 presents results for the horizontal tail off, and figures 25 and 26, low-speed results with the tail on. Figure 27 presents data showing the effect of full-span flap deflection on longitudinal characteristics at higher speeds; figure 28, the corresponding effect of partial-span flaps and tail height. Except for data in figure 27, the results presented in figures 21 through 32 are from the second phase of the test.

Balanced conditions.- Some data were obtained with essentially zero drag and moment, and a specified value of lift. Figure 29 presents data showing the variation of angle of attack, lift, fan RPM, exit-vane angle, tail incidence, and reaction control with airspeed for these balanced conditions. The flight sequences presented in figure 29 were not intended to be optimum. Figure 30 shows the control effectiveness of the horizontal tail, mounted in the mid-position, with the reaction control operating. Figure 31 presents longitudinal characteristics with exit vanes deflected to provide a propulsive force. While these data are not balanced in moment, it is believed the longitudinal stability is representative of that in balanced flight if the horizontal tail is sufficiently far from

the angle for stall. Figure 32 presents the variation of moment with airspeed for the nearly balanced conditions shown in figure 29.

Ames Research Center
National Aeronautics and Space Administration
Moffett Field, Calif., June 8, 1961.

REFERENCES

1. Hickey, David H., and Ellis, David R.: Wind-Tunnel Tests of a Semispan Wing With a Fan Rotating in the Plane of the Wing. NASA TN D-88, 1959.

2. Hickey, David H.: Preliminary Investigation of the Characteristics of a Two-Dimensional Wing and Propeller With the Propeller Plane of Rotation in the Wing-Chord Plane. NACA RM A57F03, 1957.

3. Wardlaw, R. L., and McEachern, N. V.: A Wing-Submerged Lifting Fan: Wind Tunnel Investigations and Analysis of Transition Performance. National Research Council of Canada. Aero. Rep. LR-243, April 1959.

4. Maki, Ralph L., and Hickey, David H.: Aerodynamics of a Fan-in-Fuselage Model. NASA TN D-789, 1961.

TABLE I.- COORDINATES OF WING AIRFOIL SECTION (NACA 63A-210) PARALLEL TO THE MODEL PLANE OF SYMMETRY

Upper surface		Lower surface	
x/c	z/c	x/c	z/c
0	0	0	0
.00423	.00868	.00577	-.00756
.00664	.01058	.00836	-.00900
.01151	.01367	.01349	-.01125
.02384	.01944	.02616	-.01522
.04869	.02769	.05131	-.02047
.07364	.03400	.07636	-.02428
.09863	.03917	.10137	-.02725
.14869	.04729	.15131	-.03167
.19882	.05328	.20118	-.03468
.24898	.05764	.25102	-.03662
.29916	.06060	.30084	-.03764
.34935	.06219	.35065	-.03771
.39955	.06247	.40045	-.03689
.44975	.06151	.45025	-.03523
.49994	.05943	.50006	-.03283
.55012	.05637	.54988	-.02985
.60028	.05245	.59972	-.02641
.65041	.04772	.64959	-.02262
.70052	.04227	.69948	-.01861
.75061	.03624	.74939	-.01464
.80074	.02974	.79926	-.01104
.85072	.02254	.84928	-.00812
.90050	.01519	.89950	-.00539
.95026	.00769	.94974	-.00279
1.00000	.00021	1.00000	-.00021

Leading-edge radius 0.0077c
Slope of radius through leading edge 0.0842

TABLE II.- SINGLE-SLOTTED TRAILING-EDGE-FLAP COORDINATES PARALLEL TO THE MODEL PLANE OF SYMMETRY

Upper surface		Lower surface	
x/c	z/c	x/c	z/c
0	0	0	0
.0018	.0071	.0025	-.0042
.0062	.0120	.0050	-.0061
.0106	.0150	.0100	-.0085
.0221	.0193	.0175	-.0105
.0336	.0212	.0250	-.0115
.0460	.0221	.0325	-.0118
.0902	.0219	.0400	-.0115
.0990	.0217	.0493	-.0110
.1080	.0210	.0993	-.0081
.1505	.0152	.1495	-.0054
.2003	.0077	.1997	-.0028
.2500	.0002	.2500	-.0002

TABLE III.- FAN INLET COORDINATES

h, in.	Section B-B	[1]Section C-C	[1]Section D-D
	r, in.	r, in.	r, in.
0	44.18	38.05	36.53
.090	40.98	36.61	35.42
.450	38.36	35.34	34.25
.900	37.15	34.48	33.53
1.350	36.35	33.94	33.07
1.800	35.77	33.54	32.75
2.250	35.29	33.23	32.50
3.150	34.55	32.77	32.14
4.050	33.98	32.45	31.94
4.950	33.53	32.23	31.80
7.650	32.57	31.80	31.56
10.350	31.92	31.58	-----
11.250	-----	-----	31.50
13.050	31.58	31.50	↓
14.750	31.50	31.50	

[1]See figure 5(d).

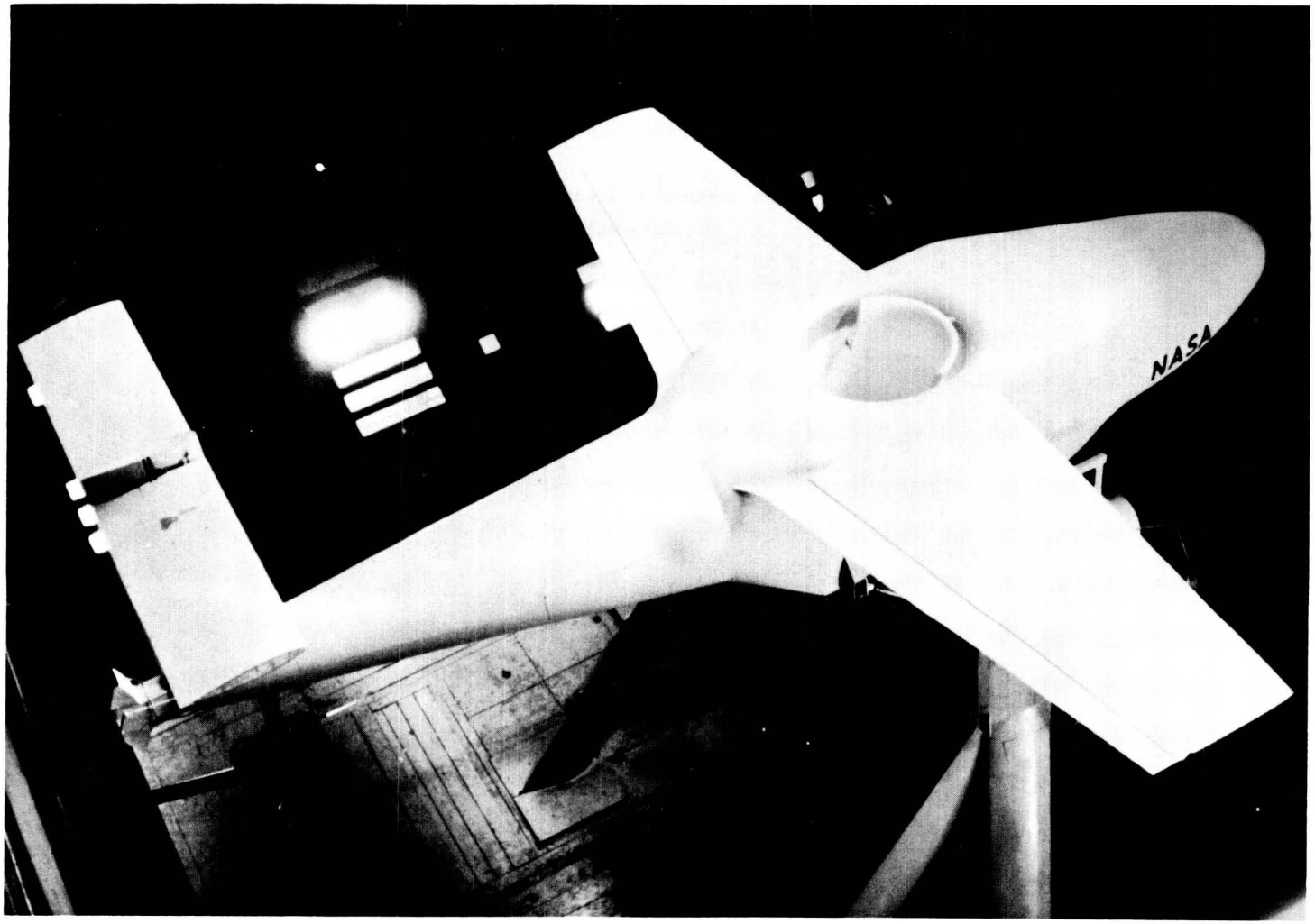

(a) Overhead view. A-26797

Figure 1.- Photographs of the model mounted in the Ames 40- by 80-Foot Wind Tunnel.

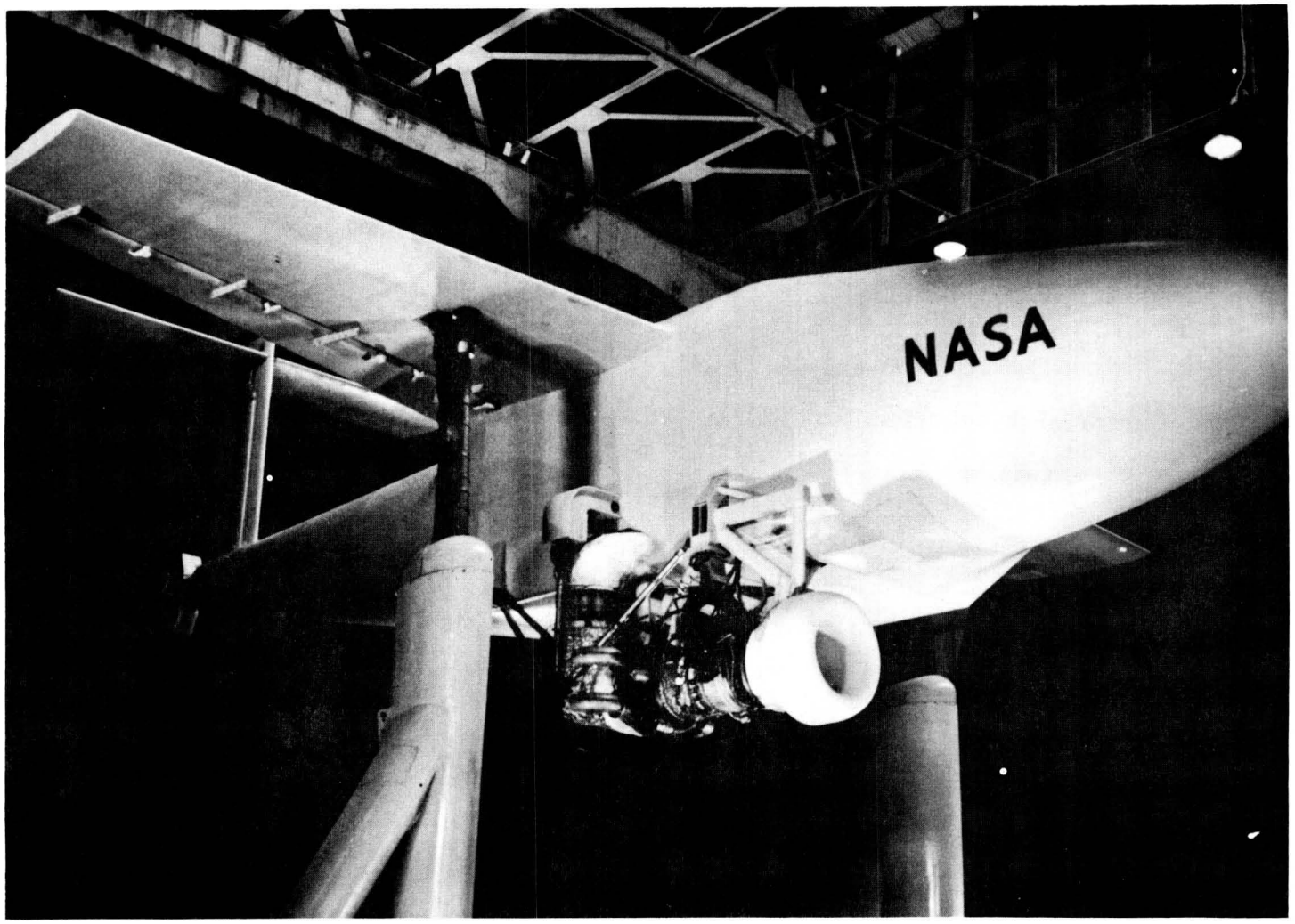

(b) Three-quarter front view. A-26798

Figure 1.- Concluded.

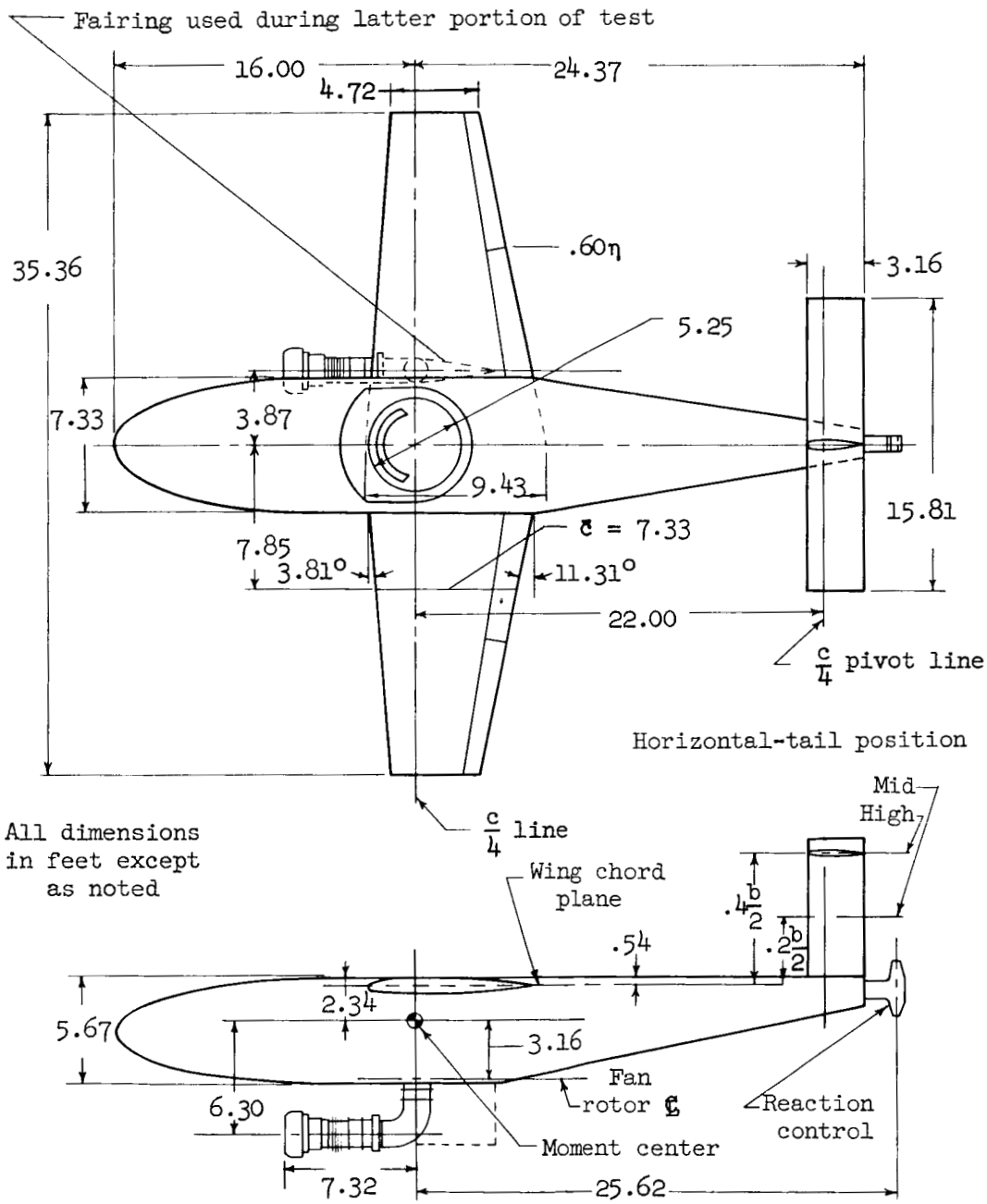

	Wing	Horizontal Tail	Vertical Tail
Area, sq ft	250	50	25
Aspect ratio	5.0	5.0	2.5
Taper ratio	0.5	1.0	1.0
Airfoil Section	NASA 63-210	NASA 63A012	NASA 63A015

Figure 2.- Geometric details of the model.

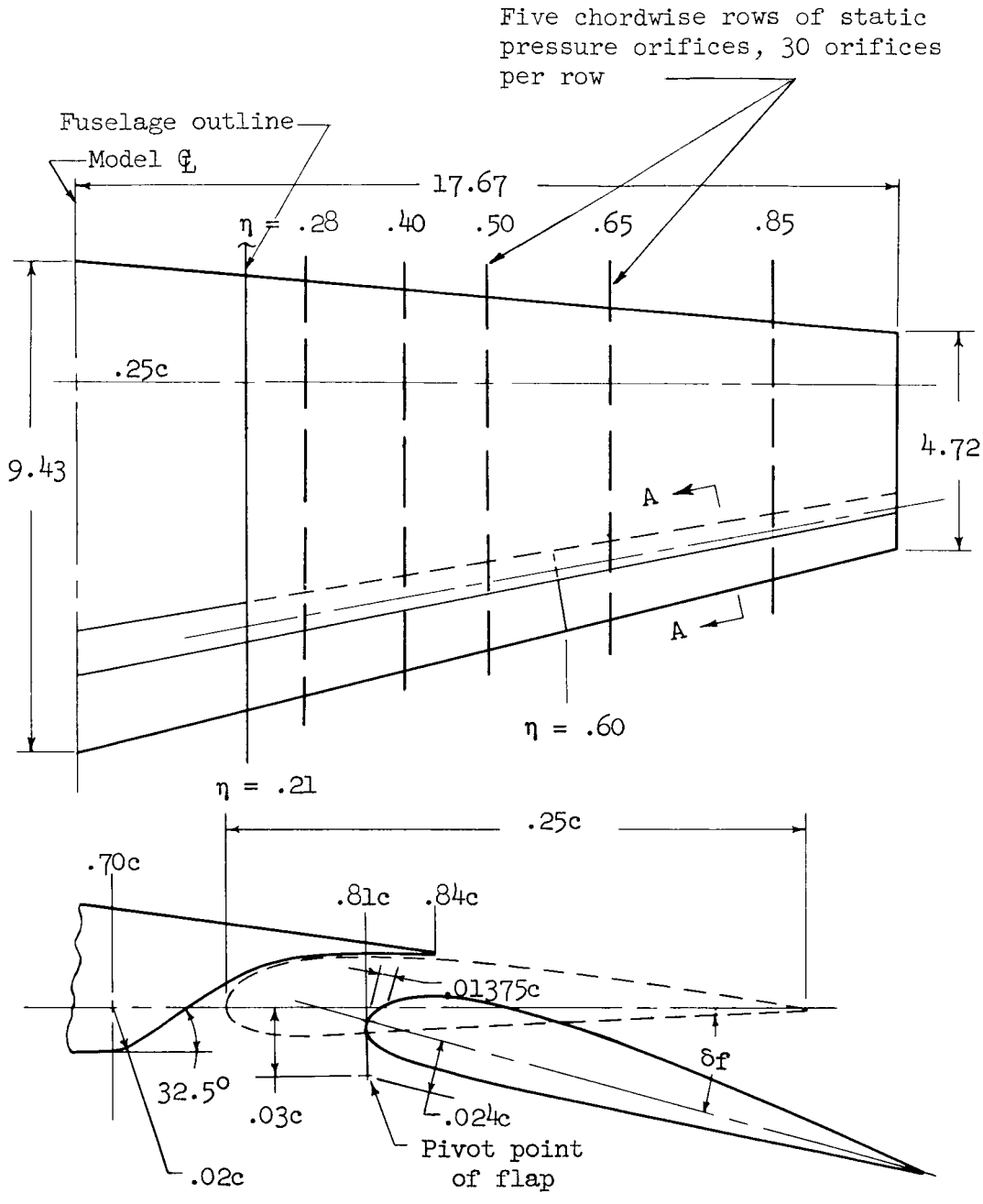

Section A-A

Figure 3.- Details of the trailing-edge flap.

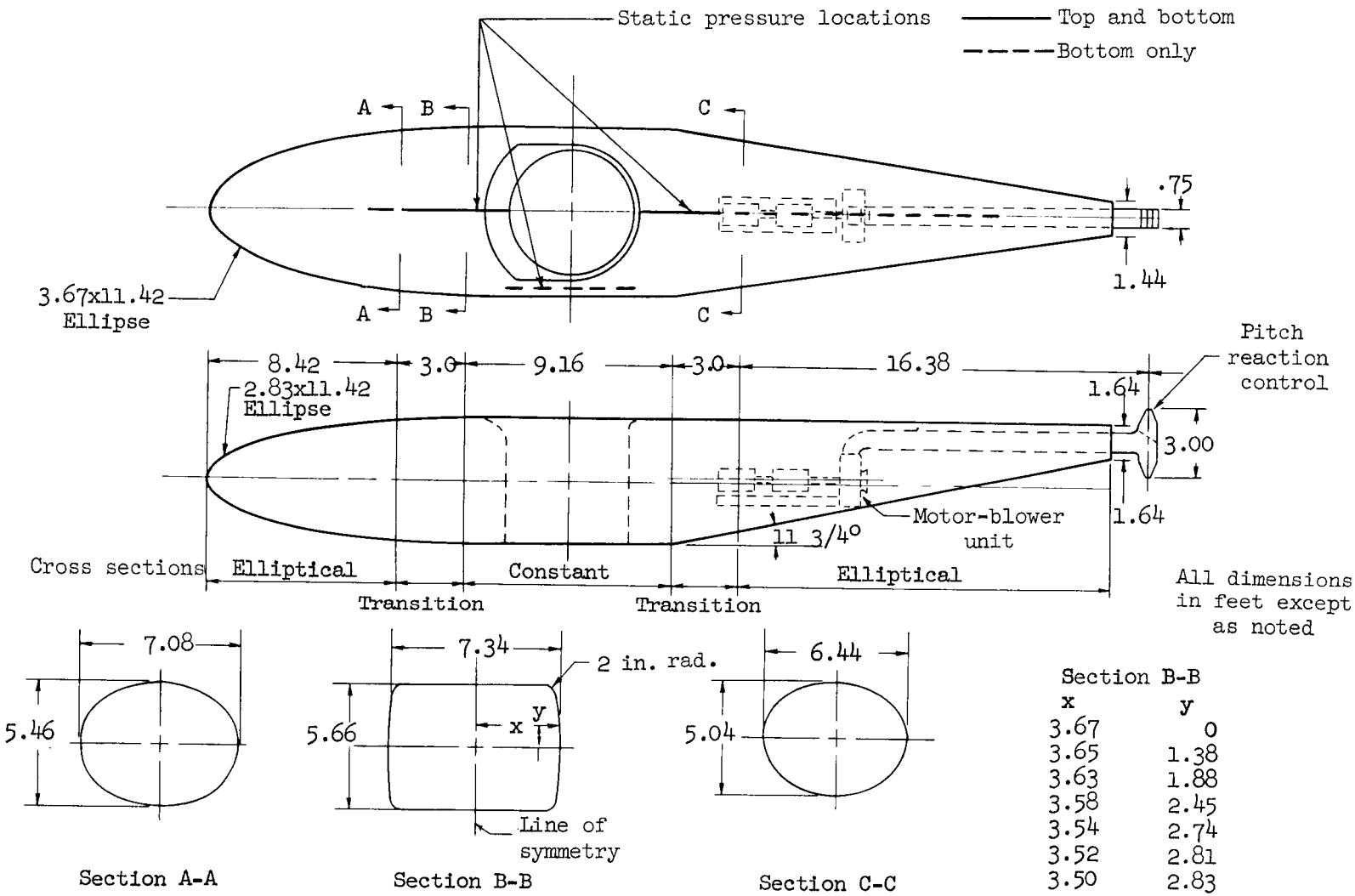

Section B-B

x	y
3.67	0
3.65	1.38
3.63	1.88
3.58	2.45
3.54	2.74
3.52	2.81
3.50	2.83

Figure 4.- Details of the fuselage and reaction control installation.

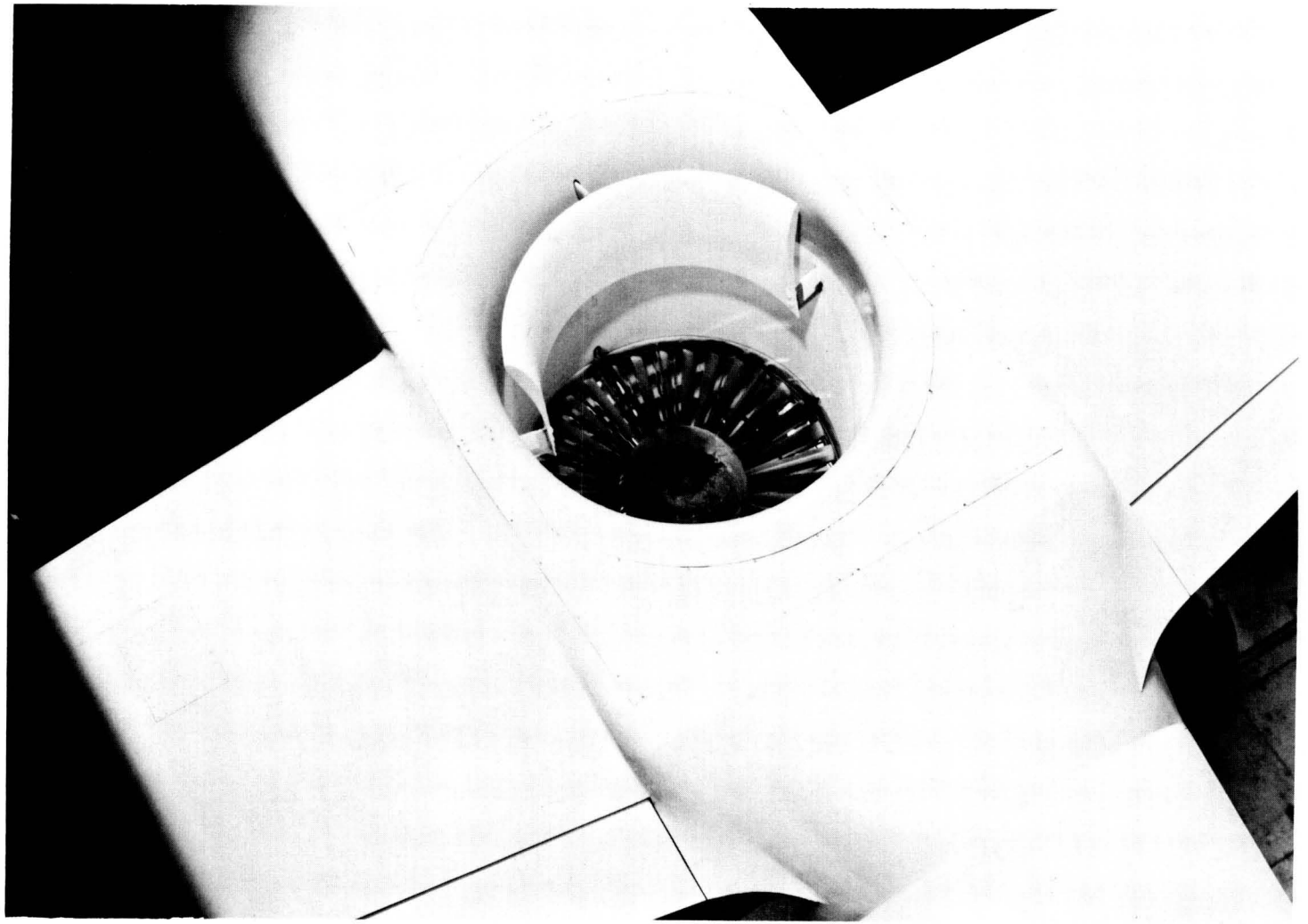

(a) View of fan inlet. A-26763

Figure 5.- Details of the fan installation.

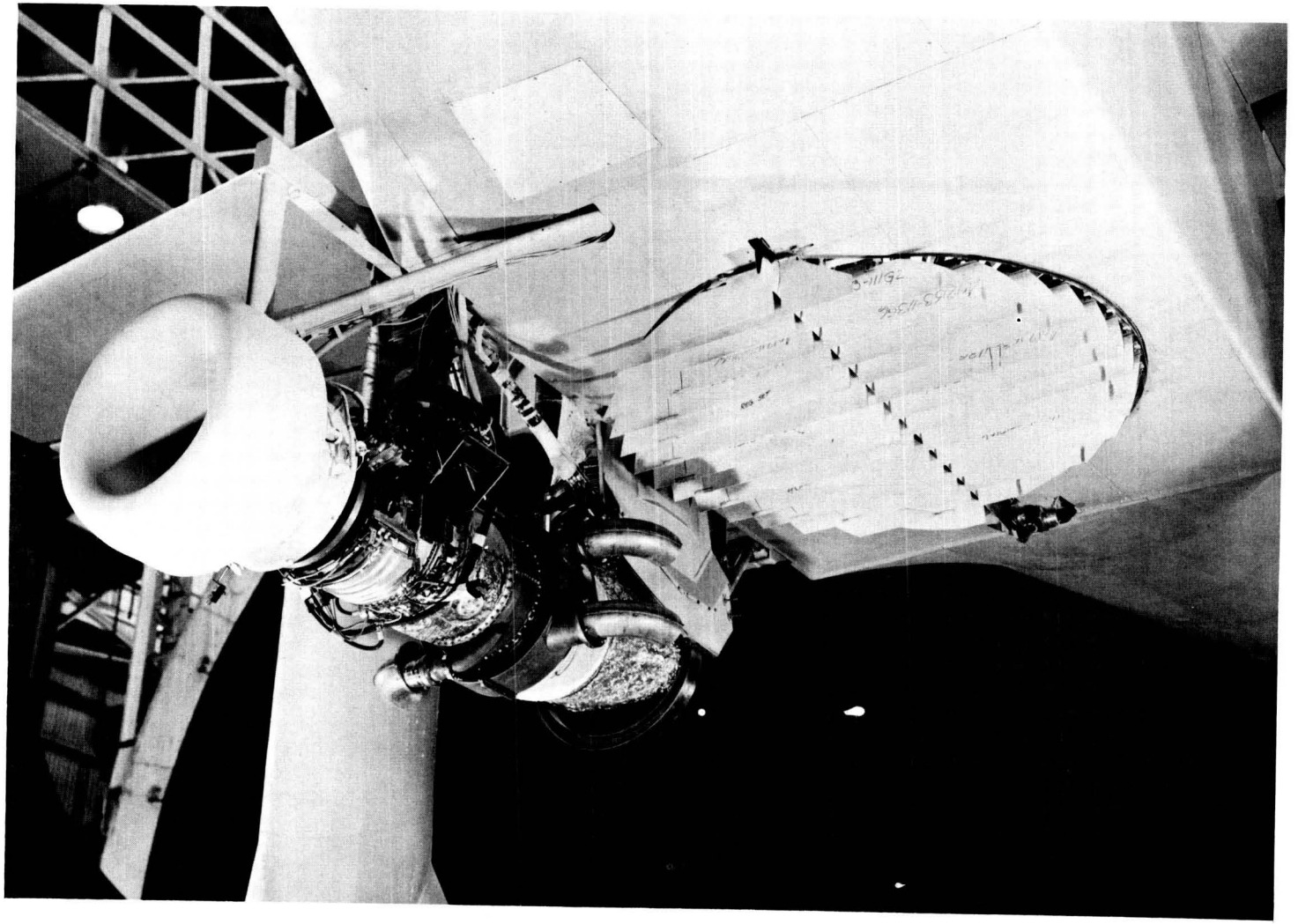

(b) View of fan exit and gas generator installation. A-26764

Figure 5.- Continued.

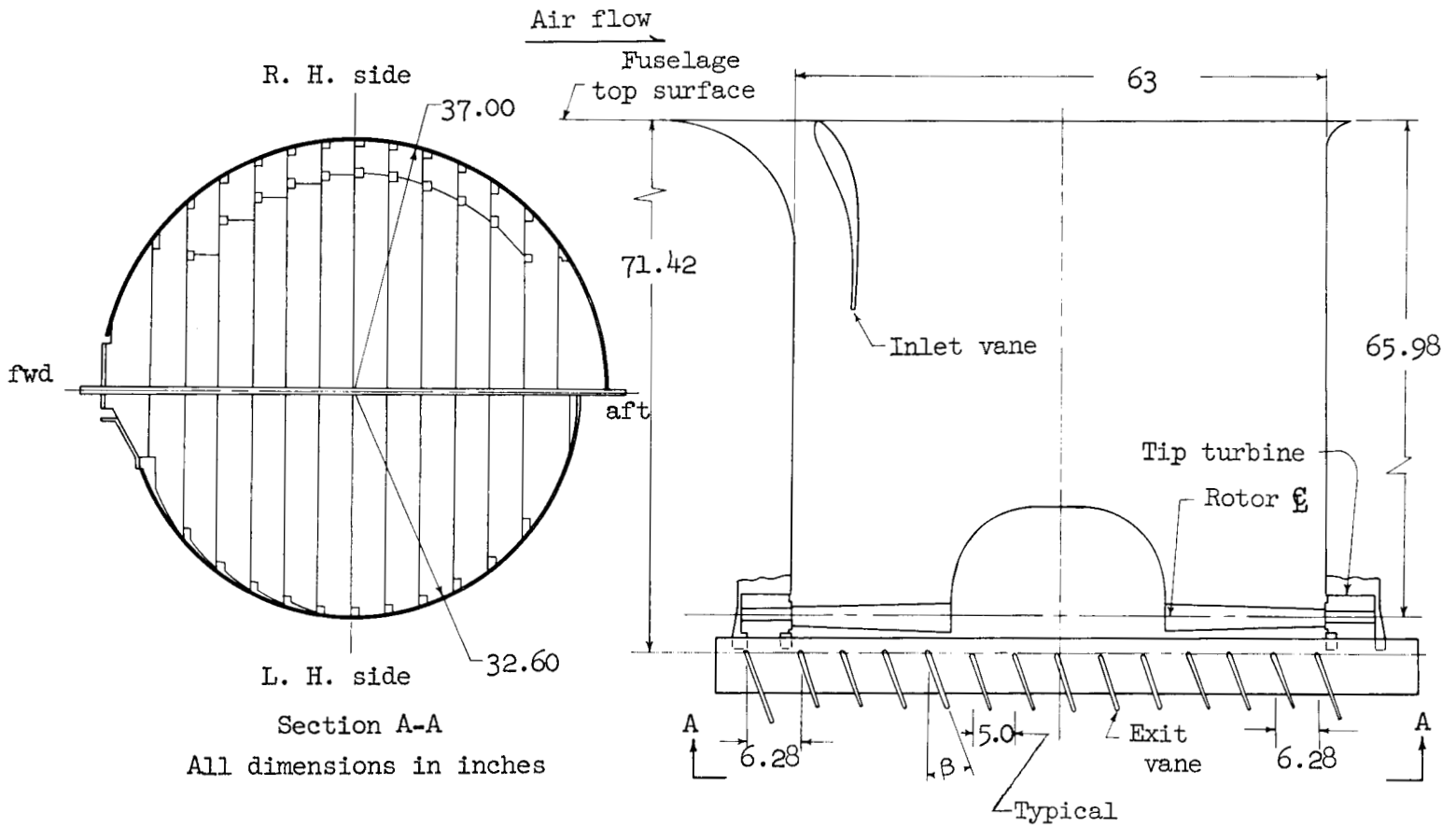

(c) Inlet duct and exit vane arrangement.

Figure 5.- Continued.

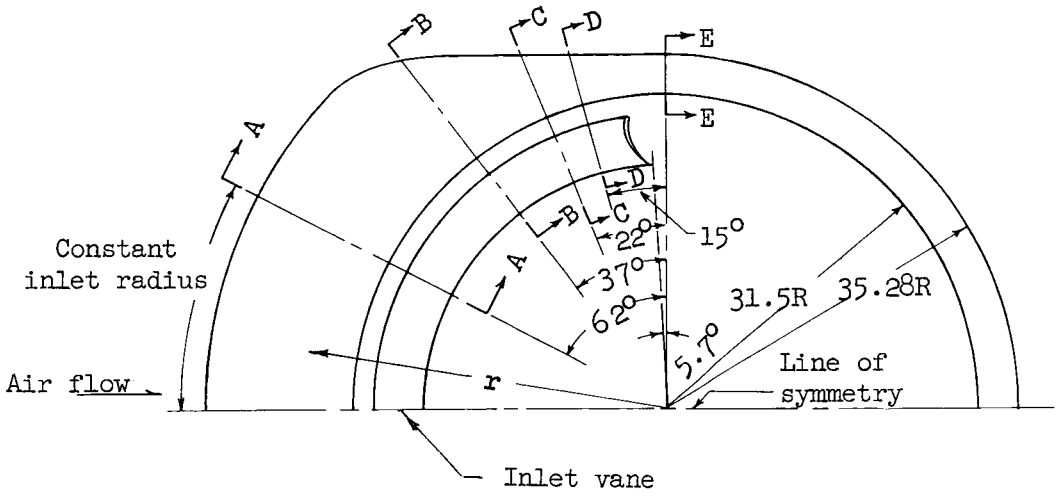

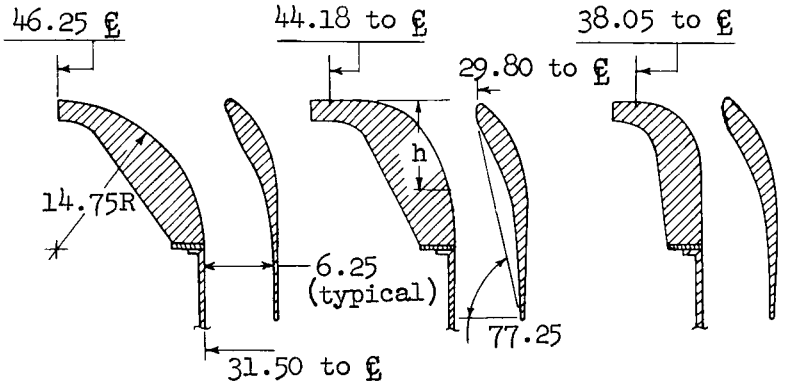

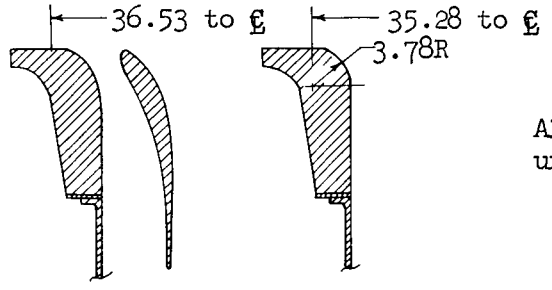

All dimensions in inches, unless otherwise noted

See table III for coordinates

(d) Details of inlet and inlet vane.

Figure 5.- Concluded.

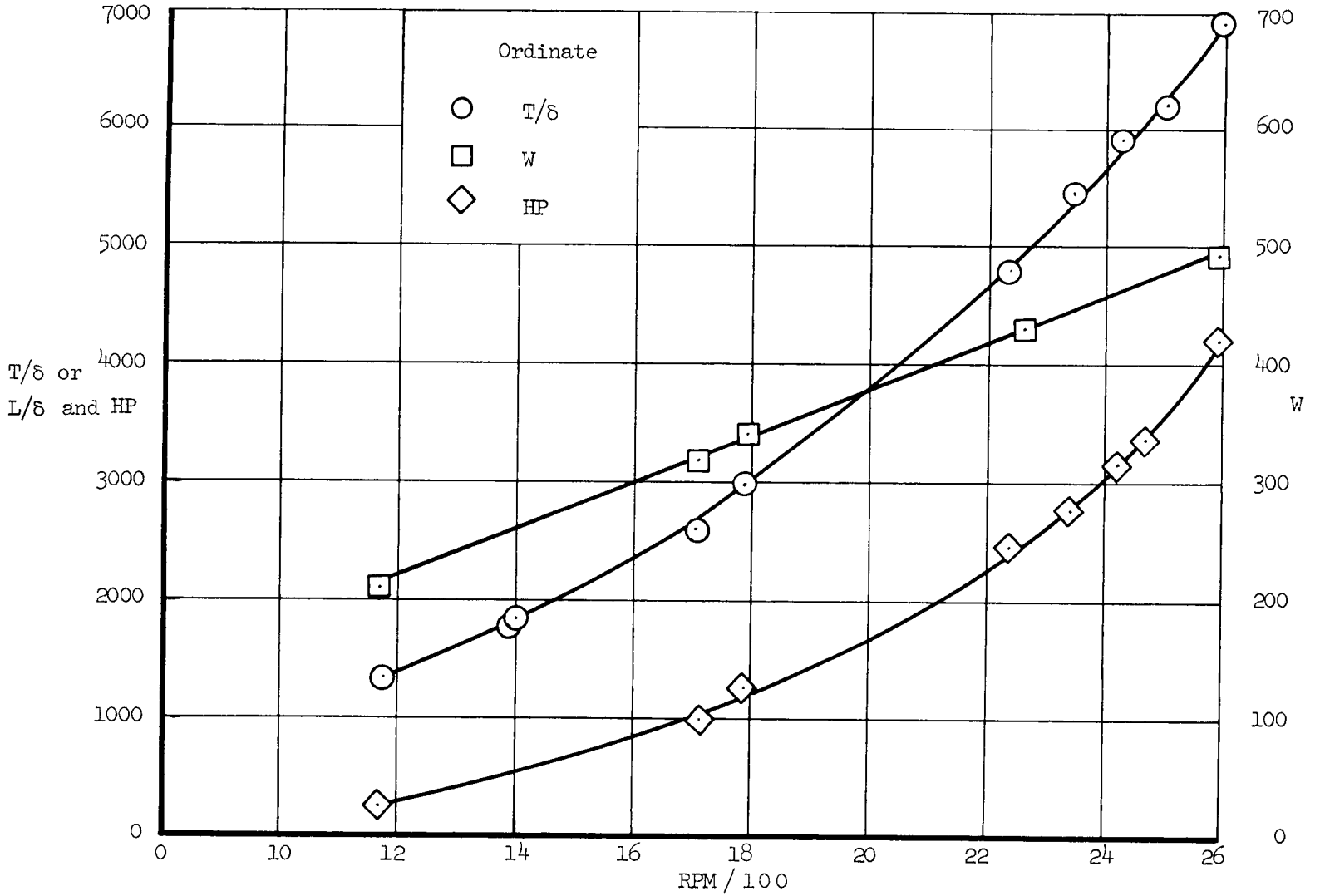

Figure 6.- Zero airspeed performance characteristics of the fan; $\alpha = 0^{\circ}$, $\beta = 0^{\circ}$.

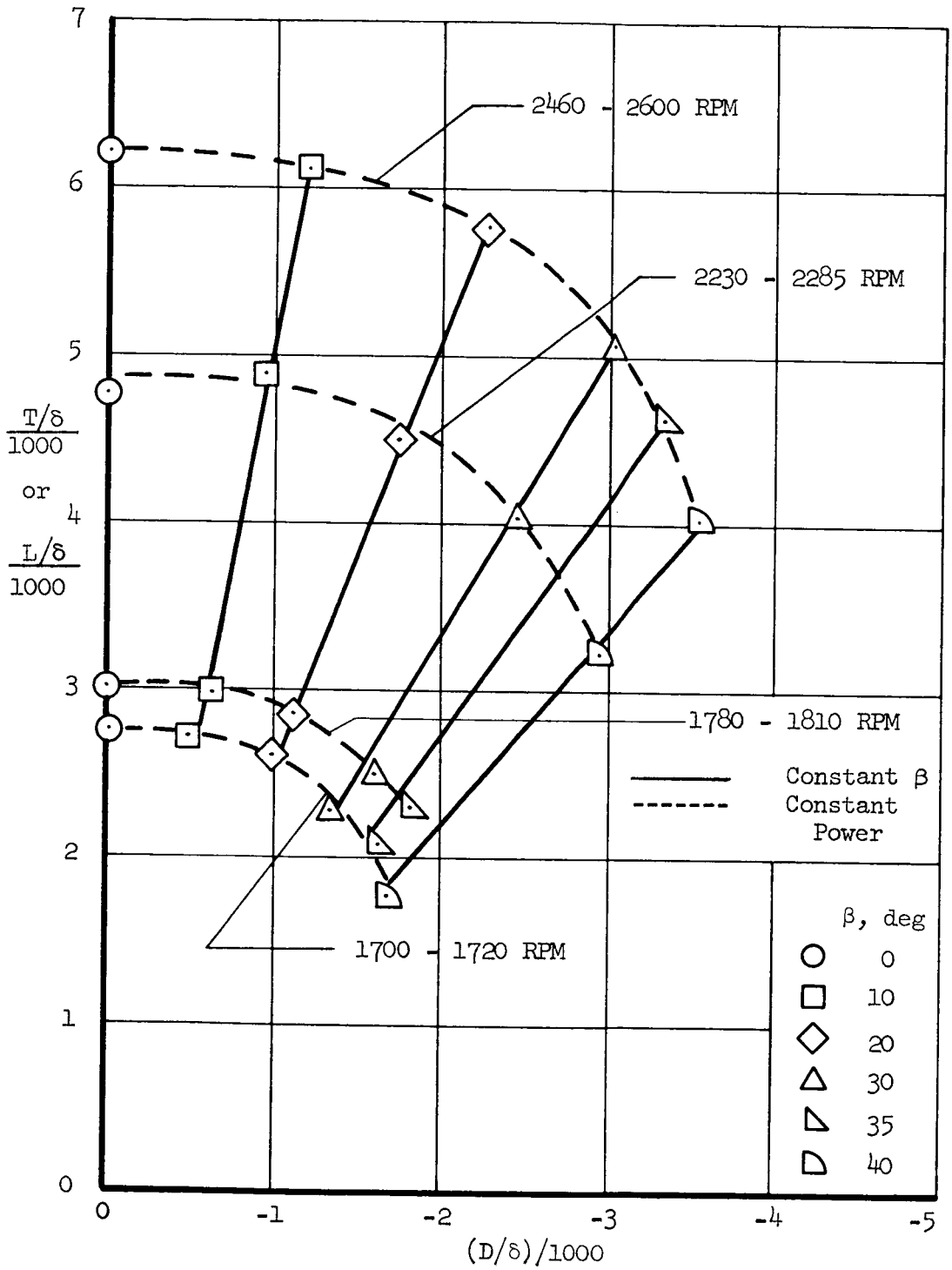

Figure 7.- Zero airspeed force characteristics of the model; $\alpha = 0^{\circ}$.

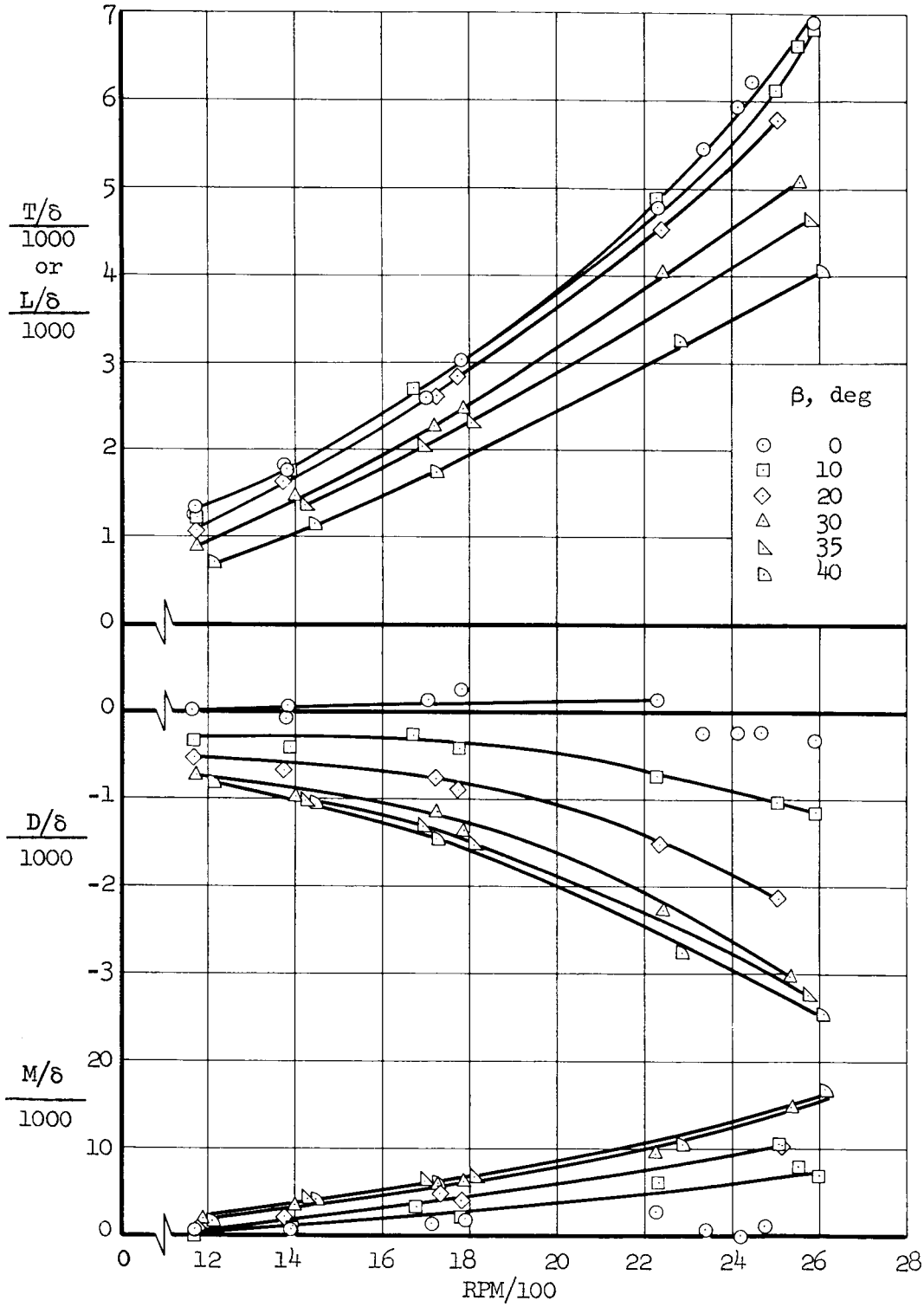

Figure 8.- Variation of forces and moments with fan RPM for several values of β, approximately zero forward speed; $\alpha = 0^{\circ}$.

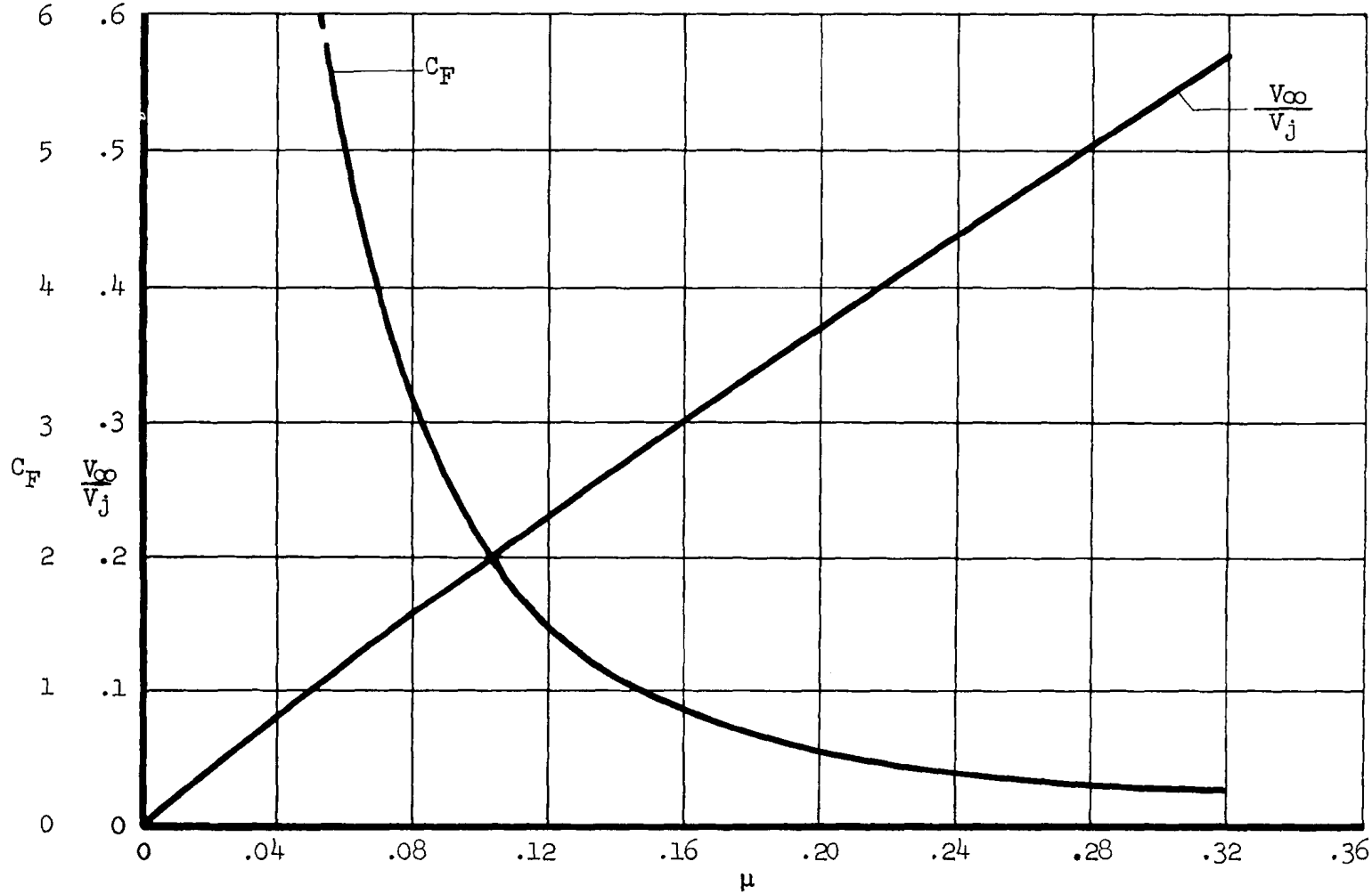

Figure 9.- The relationship between velocity ratio, thrust coefficient, and tip-speed ratio; $\alpha = 0^o$, $\beta = 0^o$.

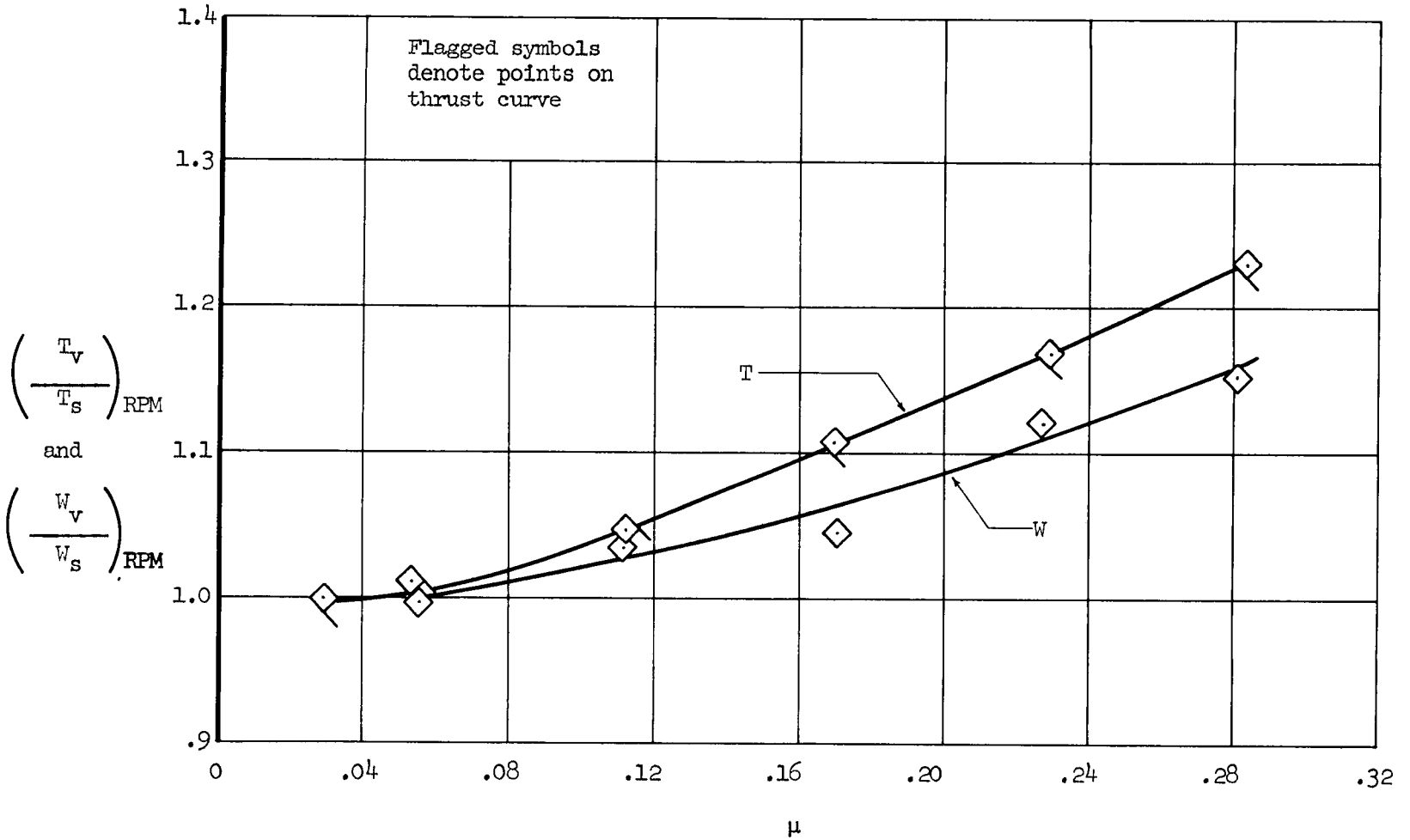

Figure 10.- The effect of airspeed (tip-speed ratio) on fan performance; $\alpha = 0^o$, $\beta = 0^o$, 2230 RPM.

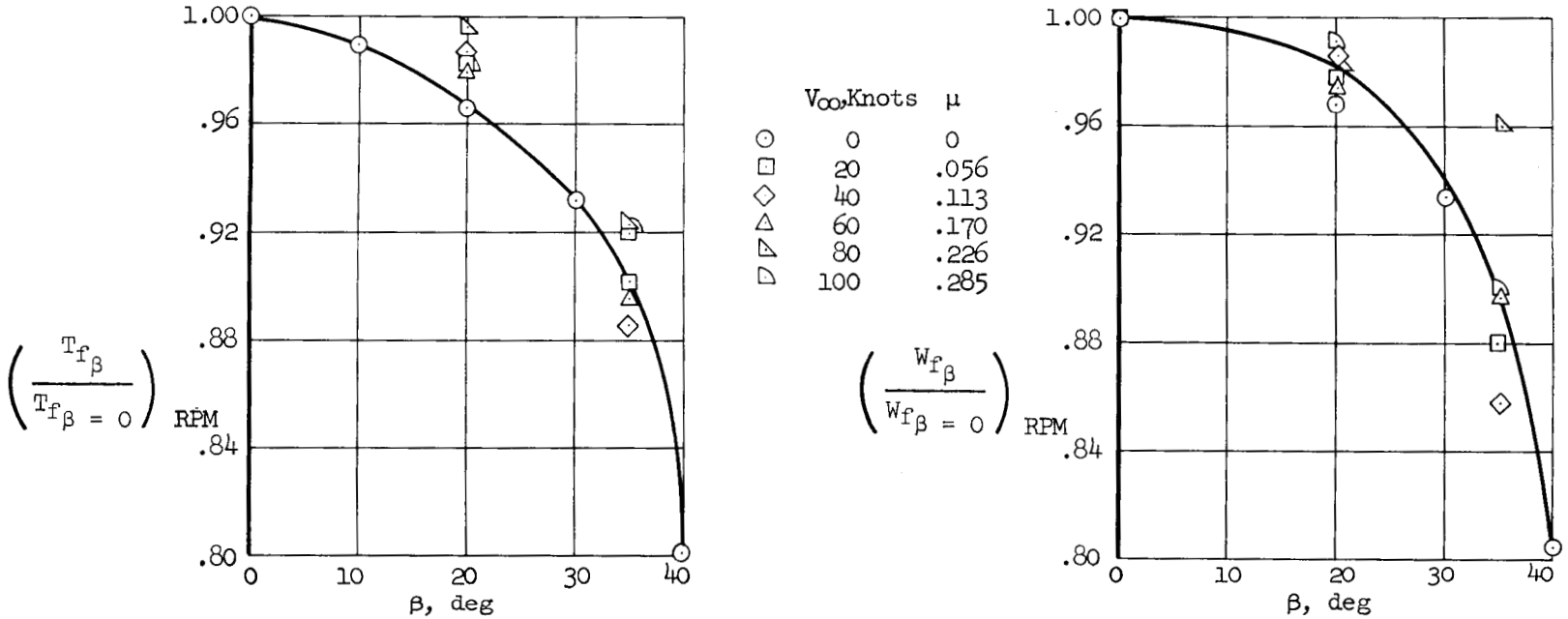

(a) Lift.

(b) Air flow.

Figure 11.- The effect of exit vane angle on fan performance at several forward speeds; $\alpha = 0^\circ$, 2150 to 2280 RPM.

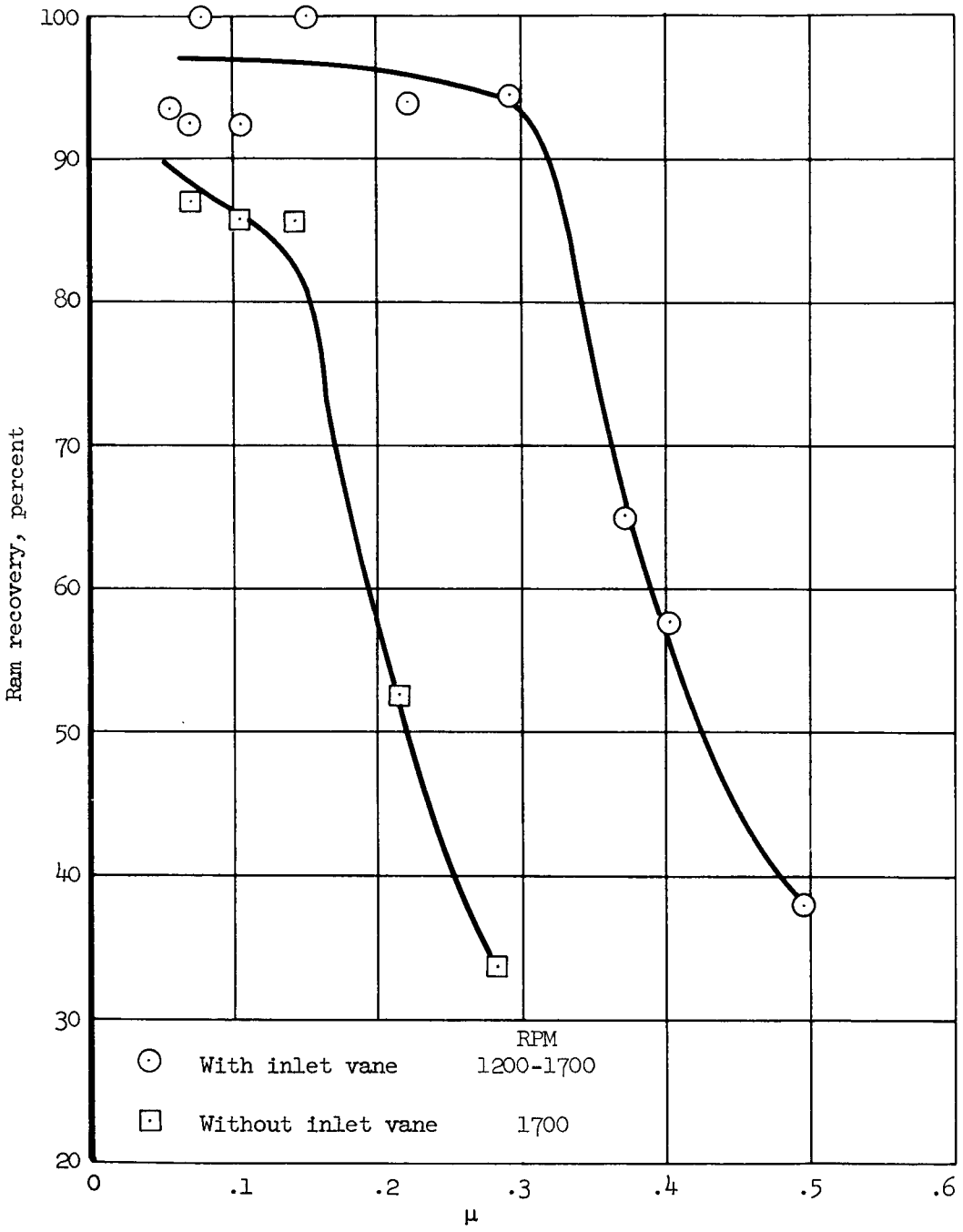

Figure 12.- The effect of forward speed (tip-speed ratio) on the fan inlet ram recovery; $\alpha = 0^{\circ}$, $\beta = 0^{\circ}$.

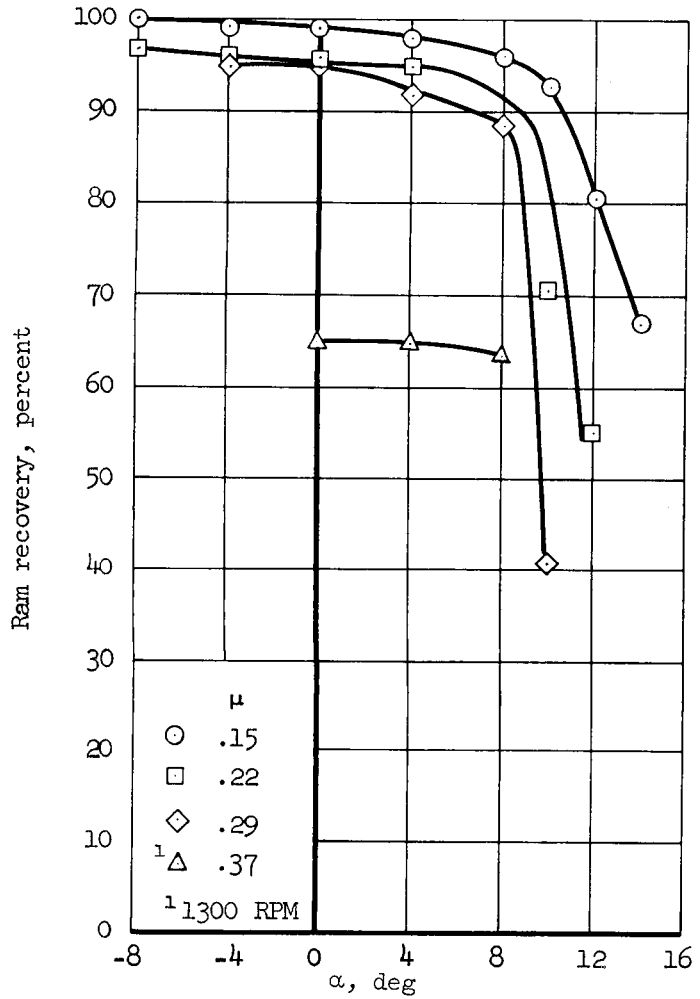

(a) With inlet vane.

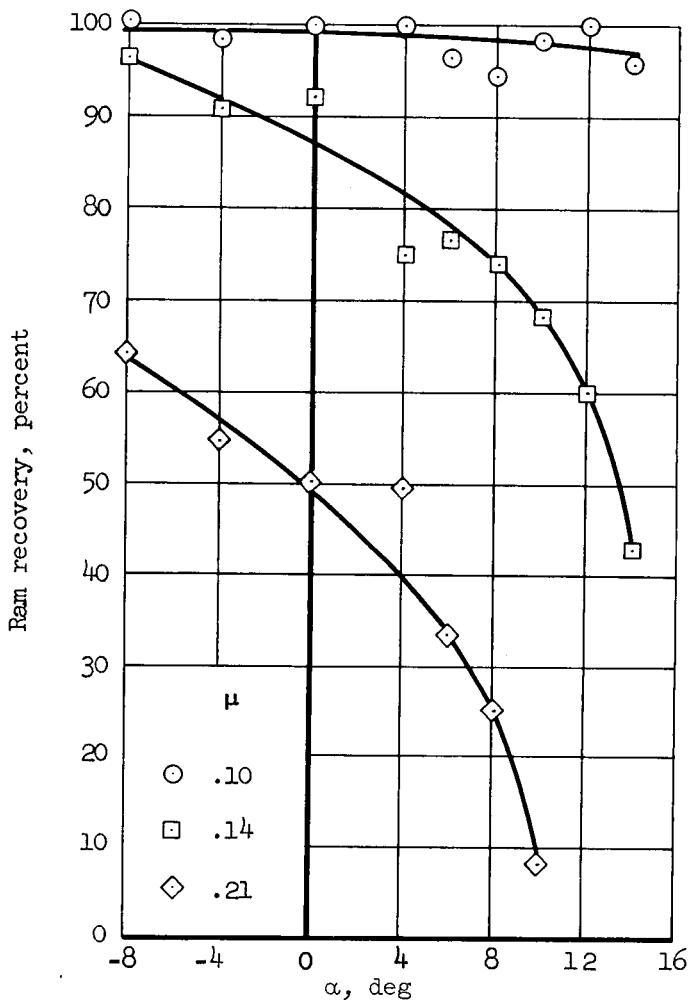

(b) Without inlet vane.

Figure 13.- The effect of angle of attack on fan inlet recovery; $\beta = 0^{\circ}$, 1650 RPM.

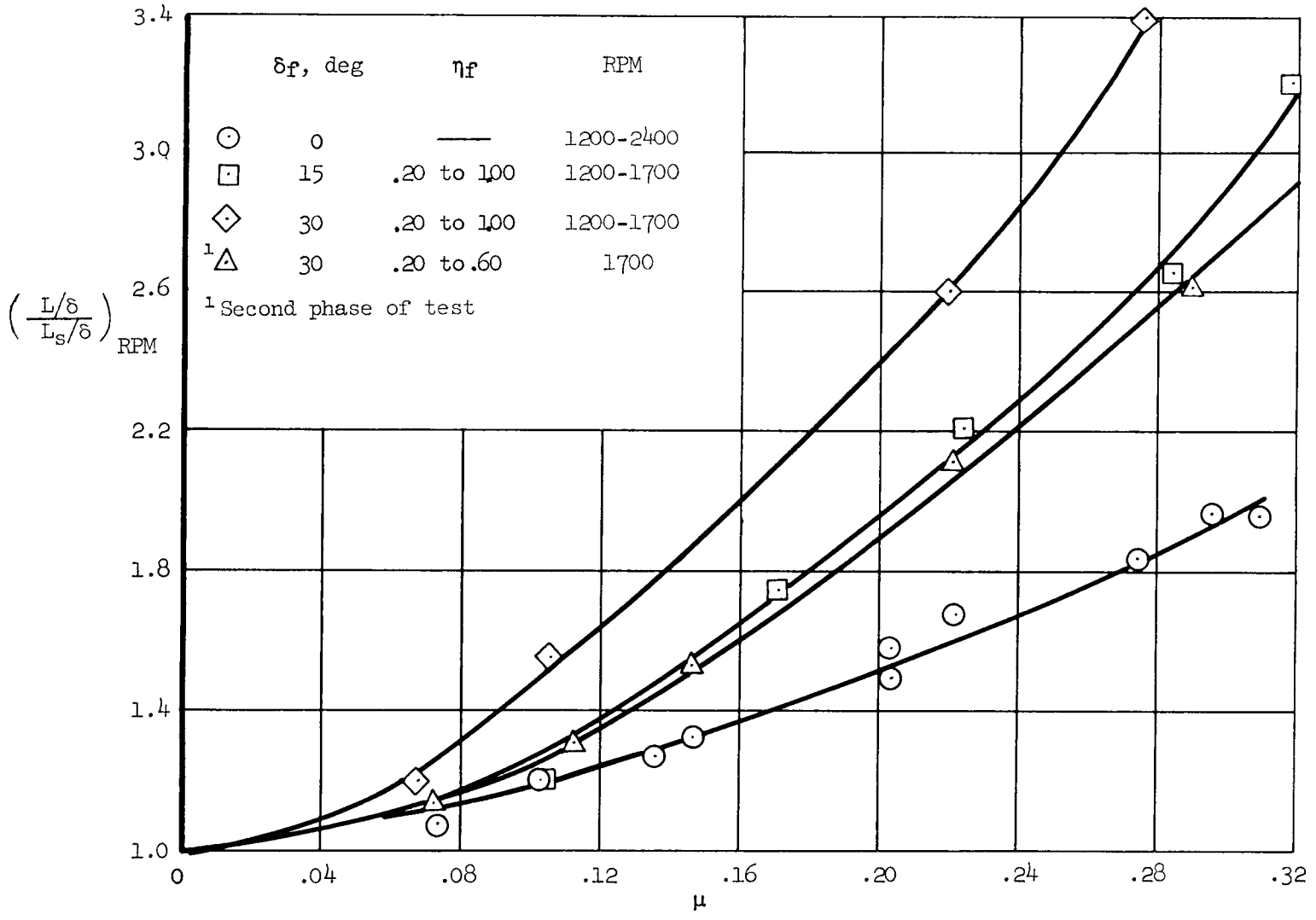

Figure 14.- The effect of forward speed on lift; $\alpha = 0^\circ$, $\beta = 0^\circ$.

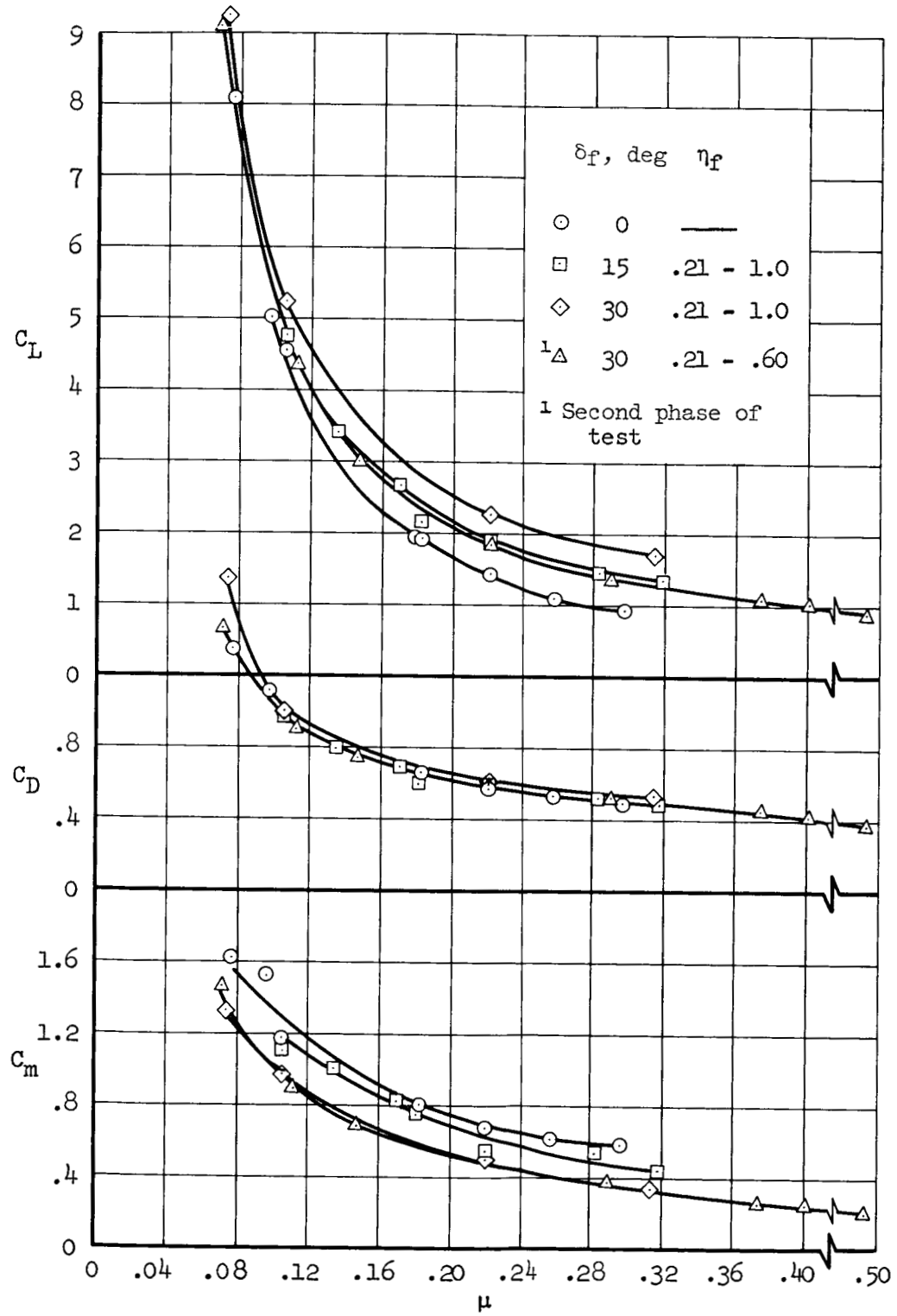

Figure 15.- Variation of longitudinal characteristics with tip-speed ratio, high horizontal-tail position; $\alpha = 0^\circ$, $\beta = 0^\circ$, 1200 to 2450 RPM.

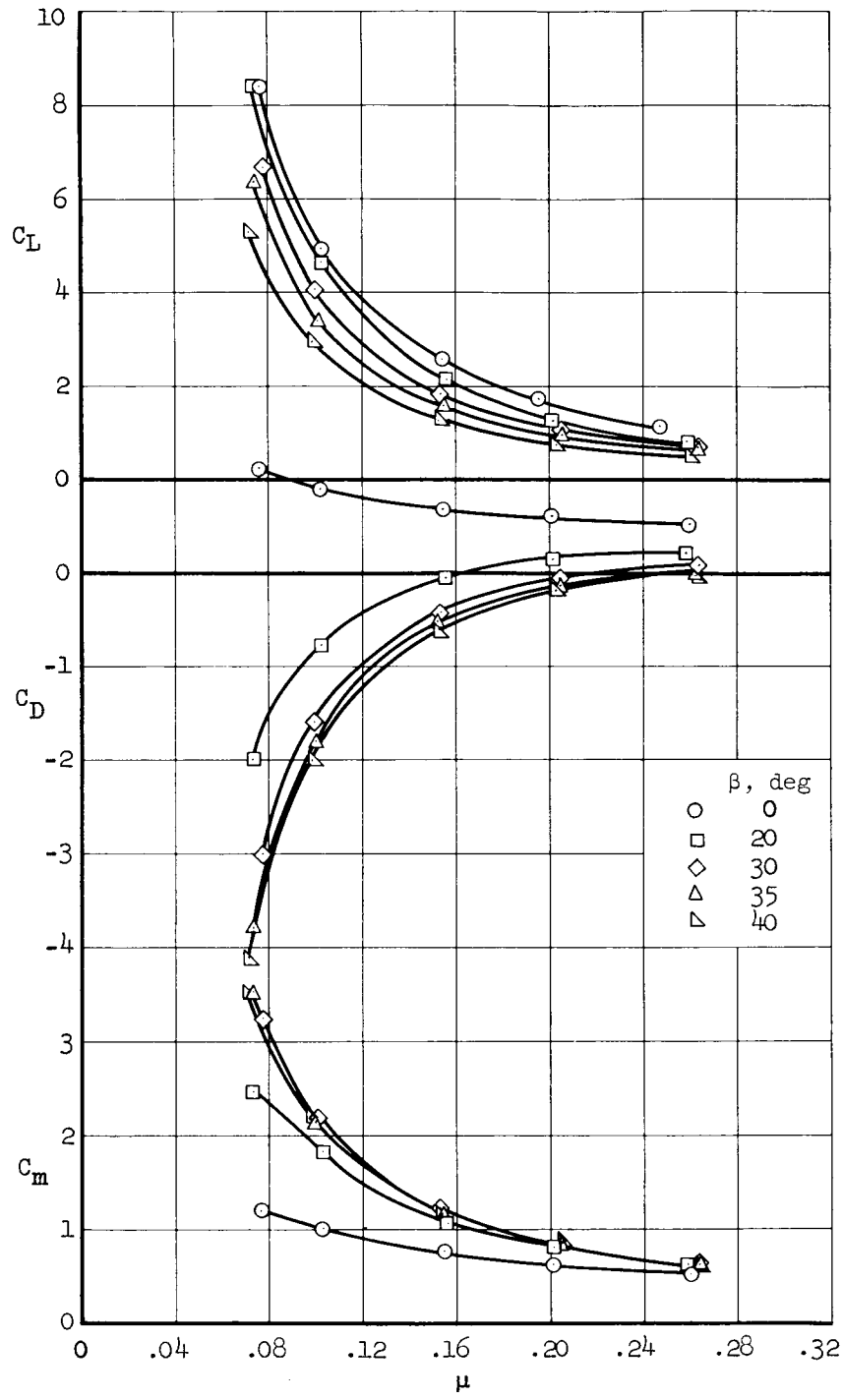

(a) Tail off, 2400 to 2550 RPM.

Figure 16.- The effect of exit vane angle and horizontal-tail position on the variation of longitudinal characteristics with tip-speed ratio; $\alpha = 0^\circ$, $\delta_f = 0^\circ$, second phase of test.

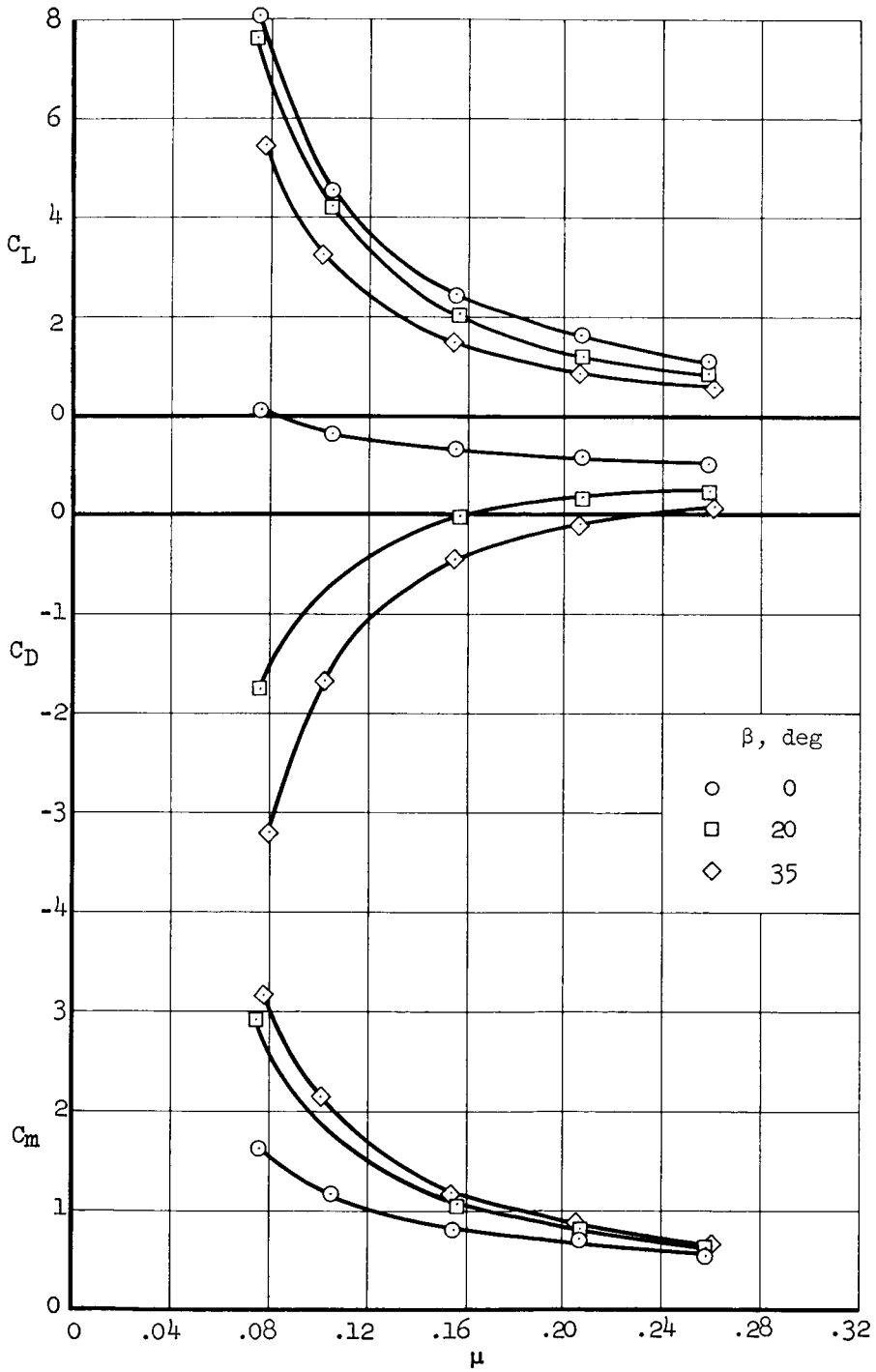

(b) High tail position, 2350 RPM.

Figure 16.- Continued.

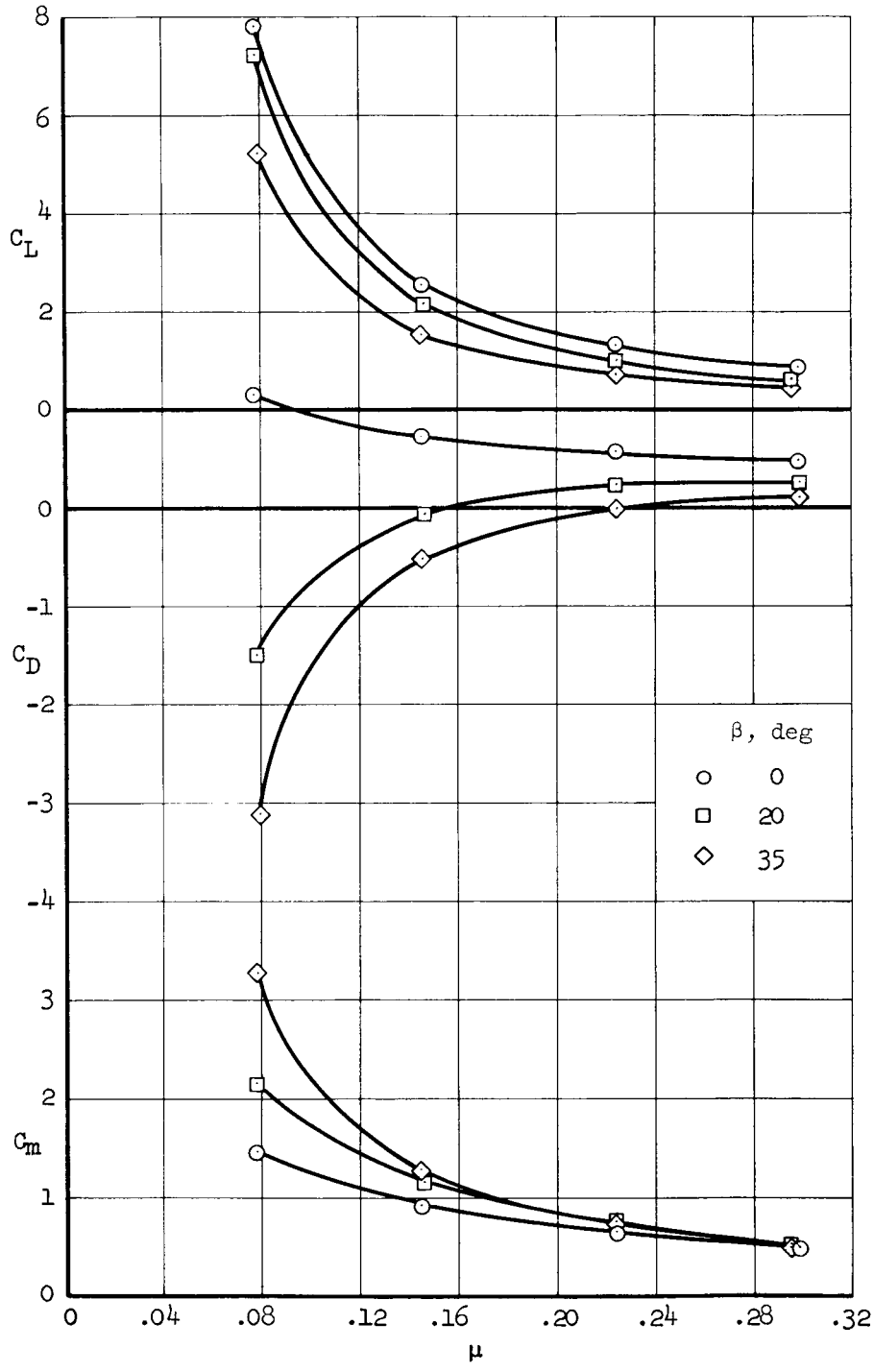

(c) Mid tail position, 1650 RPM.

Figure 16.- Concluded.

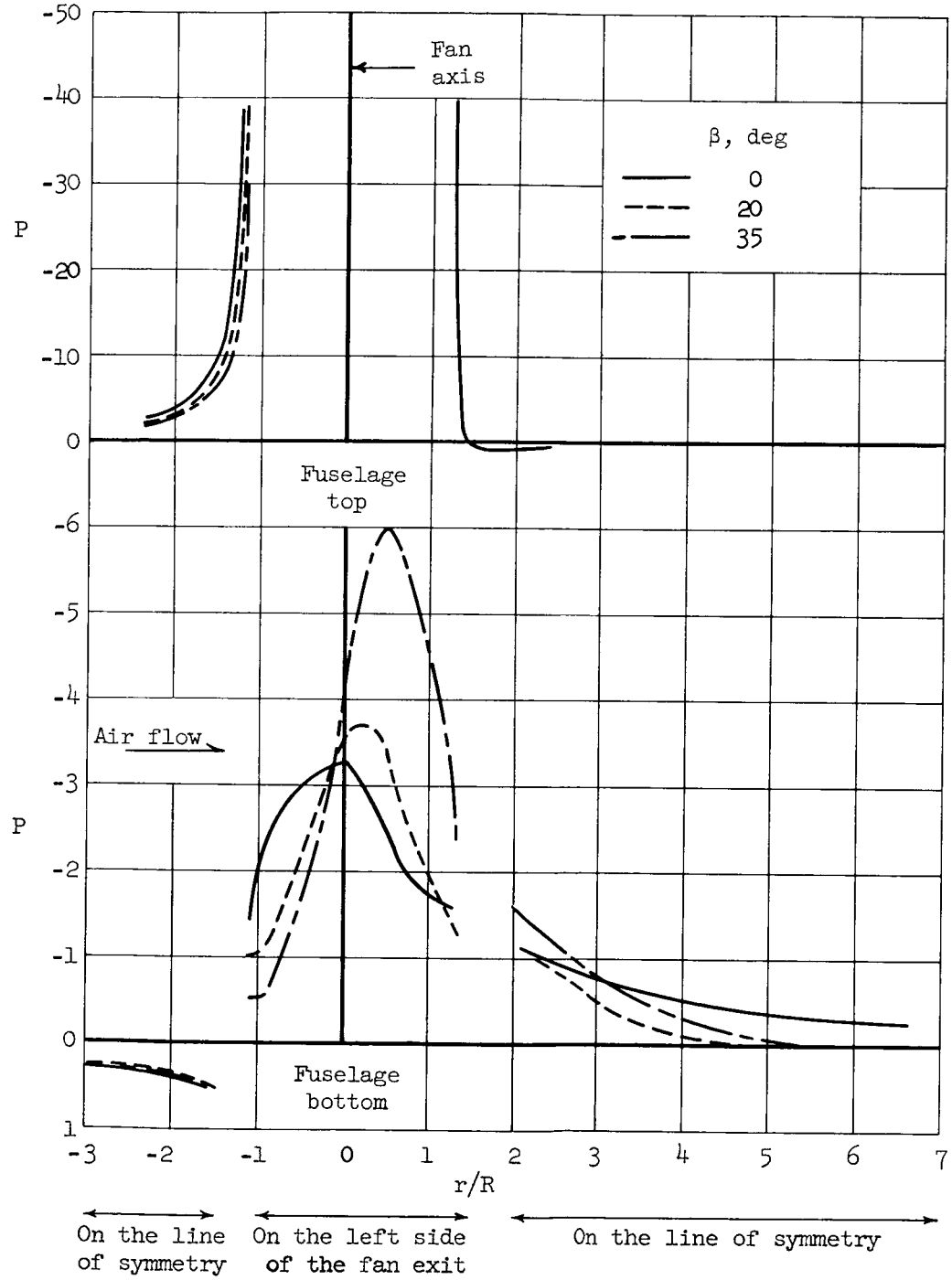

(a) $\mu = 0.076$

Figure 17.- Longitudinal pressure distributions on the fuselage for several values of tip-speed ratio and exit vane angle setting; $\alpha = 0^{\circ}$, $\delta_f = 30^{\circ}$, 1700 RPM.

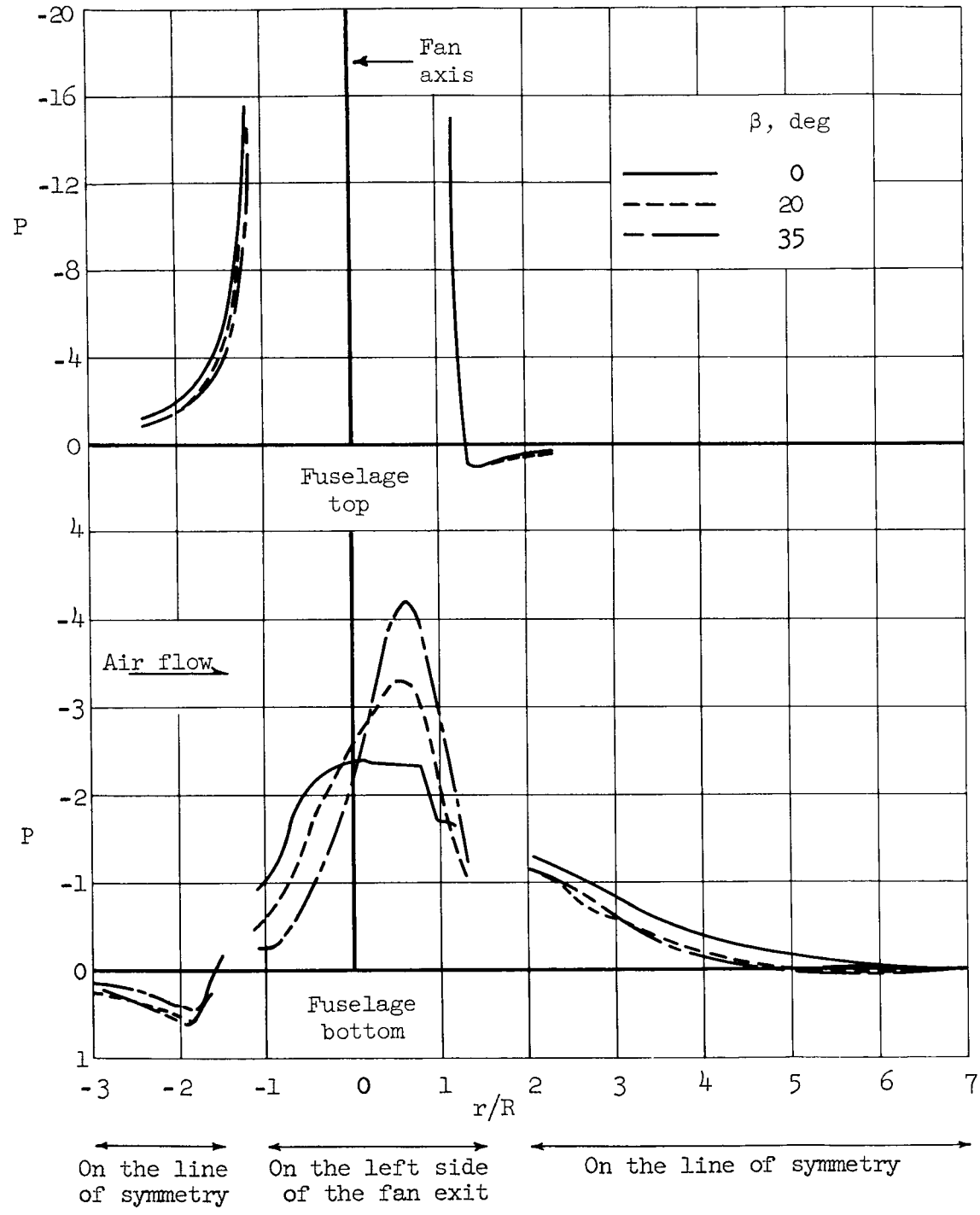

(b) $\mu = 0.145$

Figure 17.- Continued.

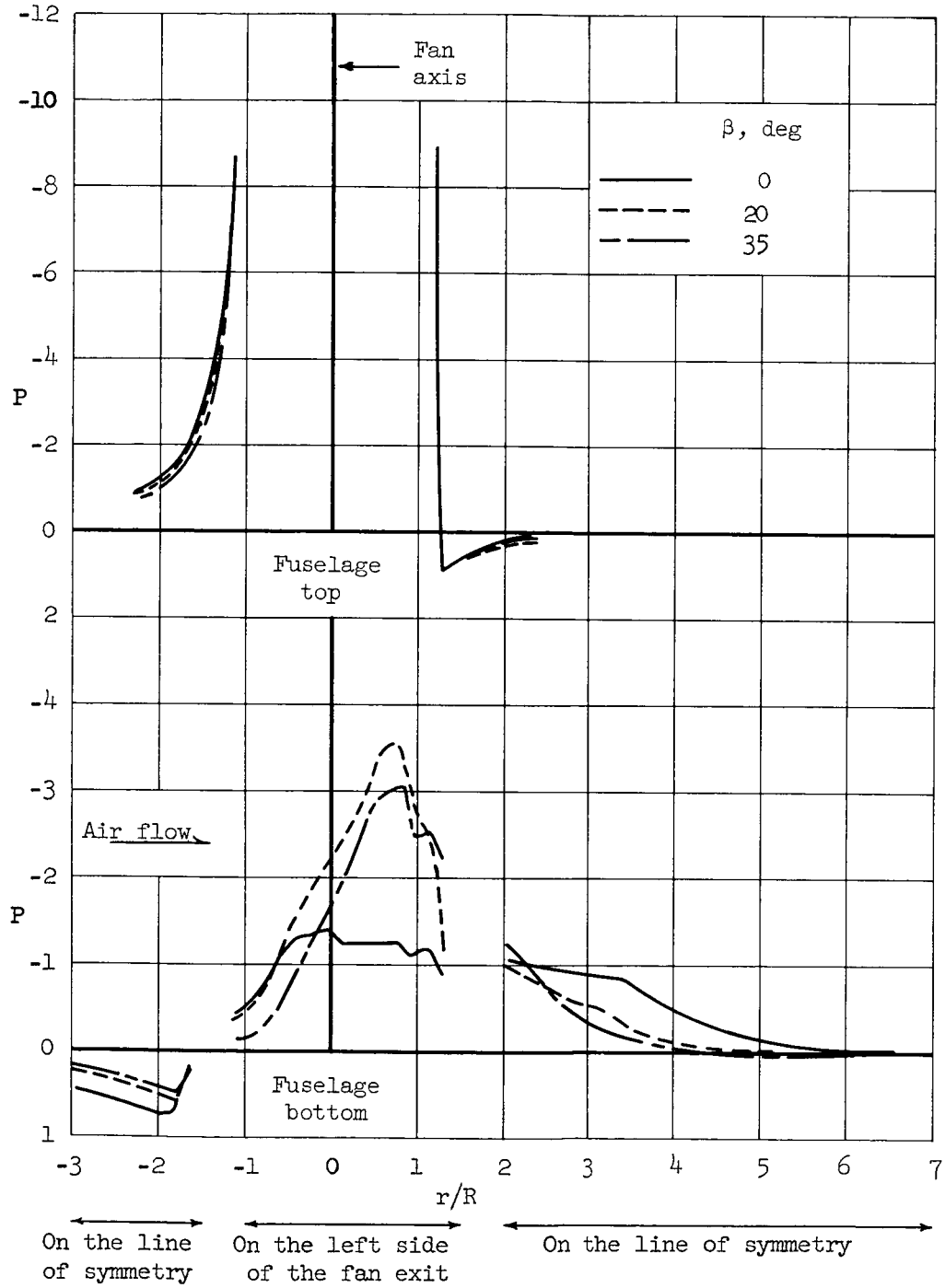

(c) $\mu = 0.224$

Figure 17.- Continued.

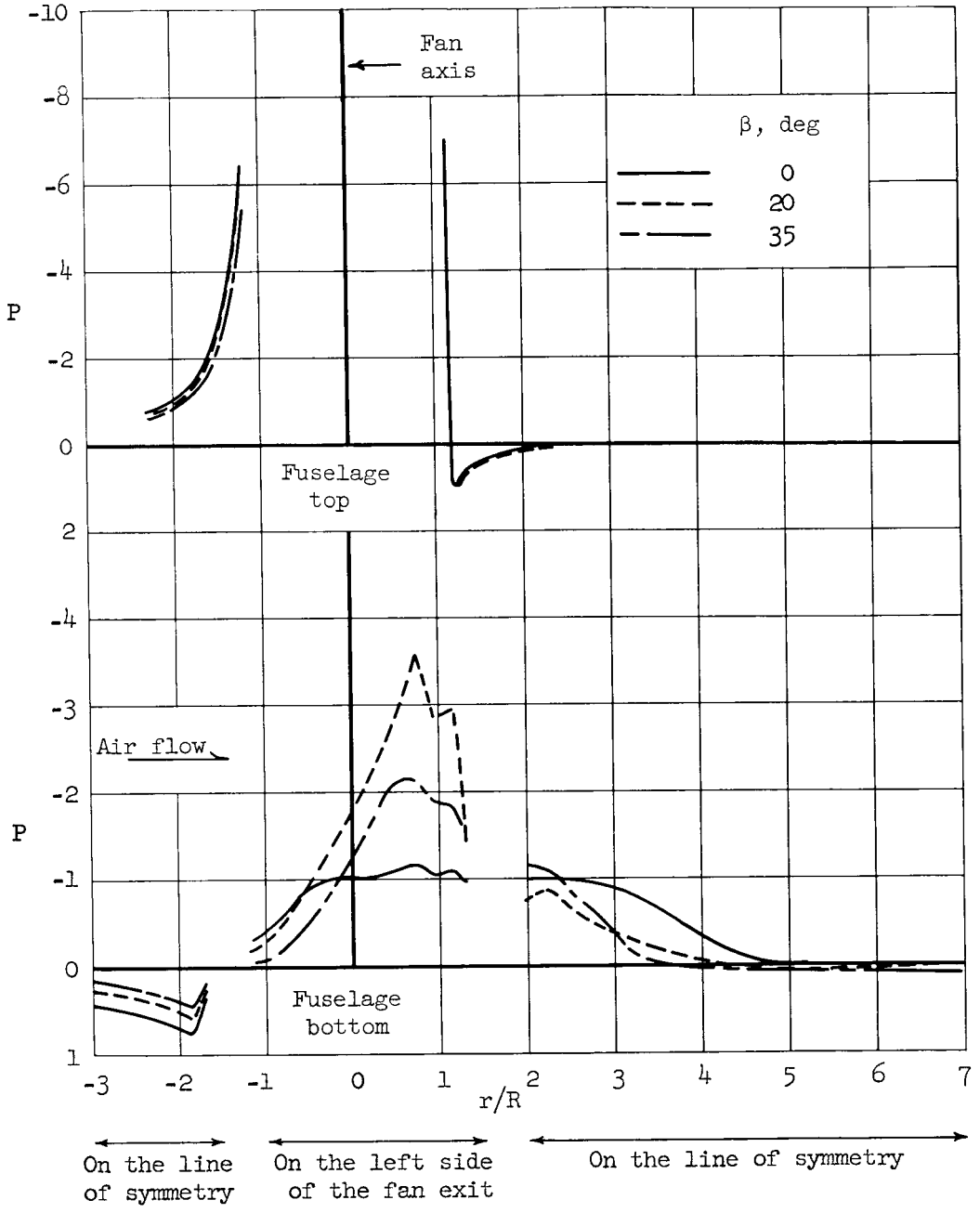

(d) $\mu = 0.295$

Figure 17.- Concluded.

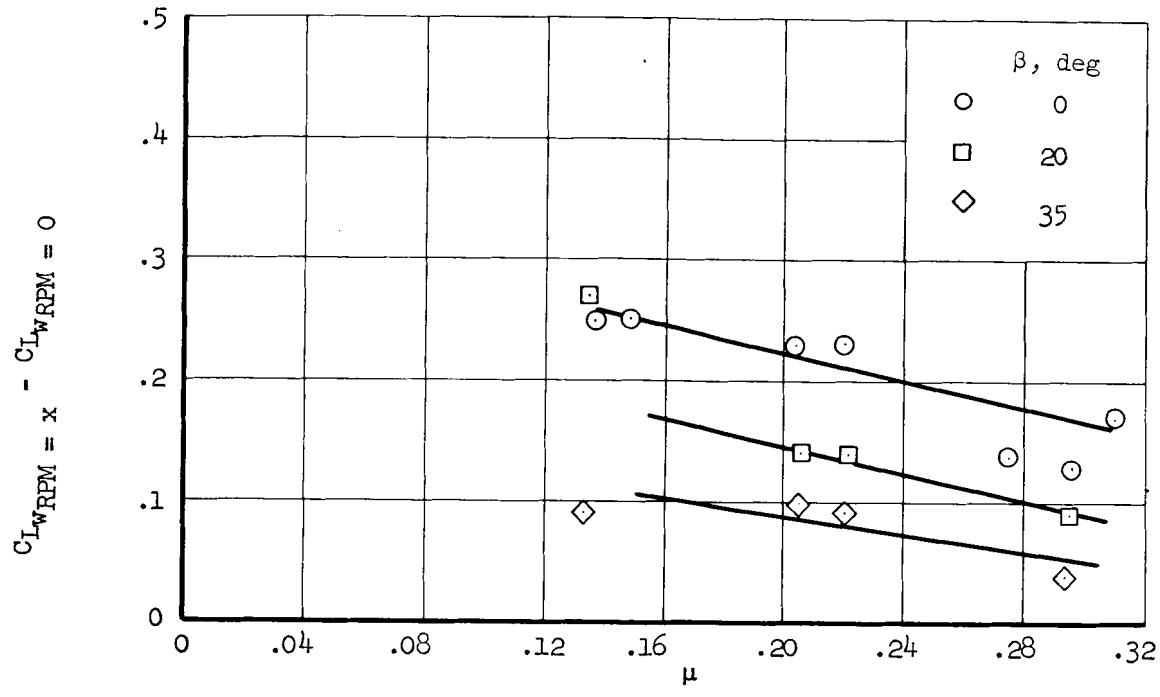

(a) Lift.

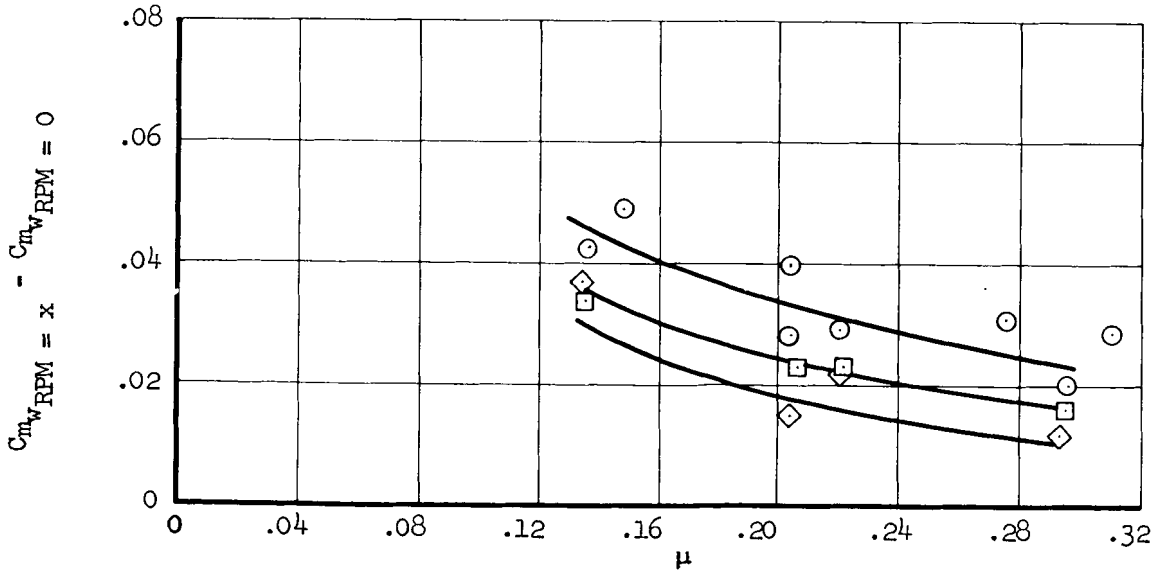

(b) Moment.

Figure 18.- Variations of measured lift and moment carried on the model wing with tip-speed ratio; $\alpha = 0^\circ$, $\beta = 0^\circ$, $\delta_f = 0^\circ$, 1200 to 1850 RPM.

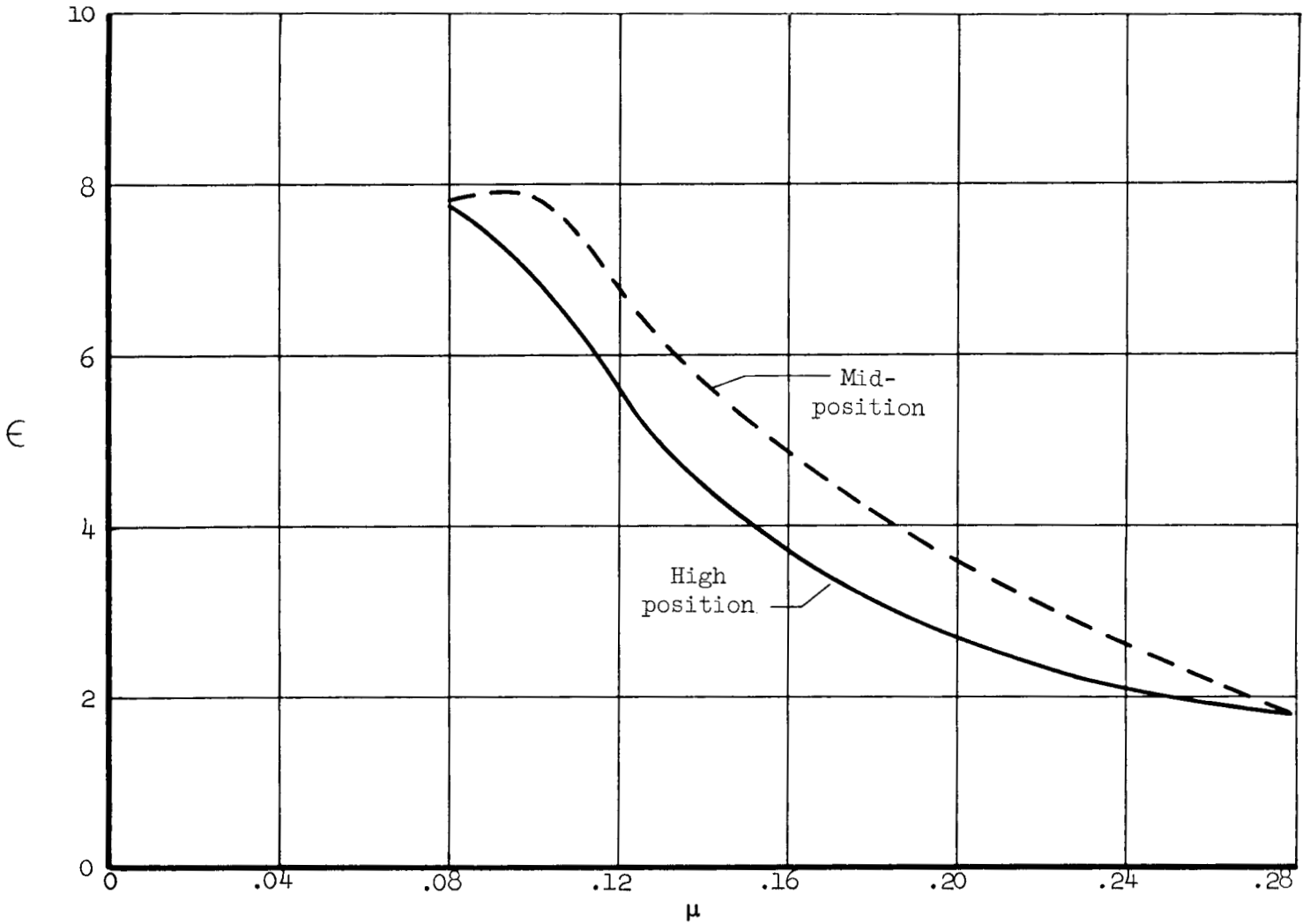

Figure 19.- The variation of average downwash at the horizontal tail with tip-speed ratio for two tail heights; $\alpha = 0^{\circ}$, $\delta_f = 0^{\circ}$.

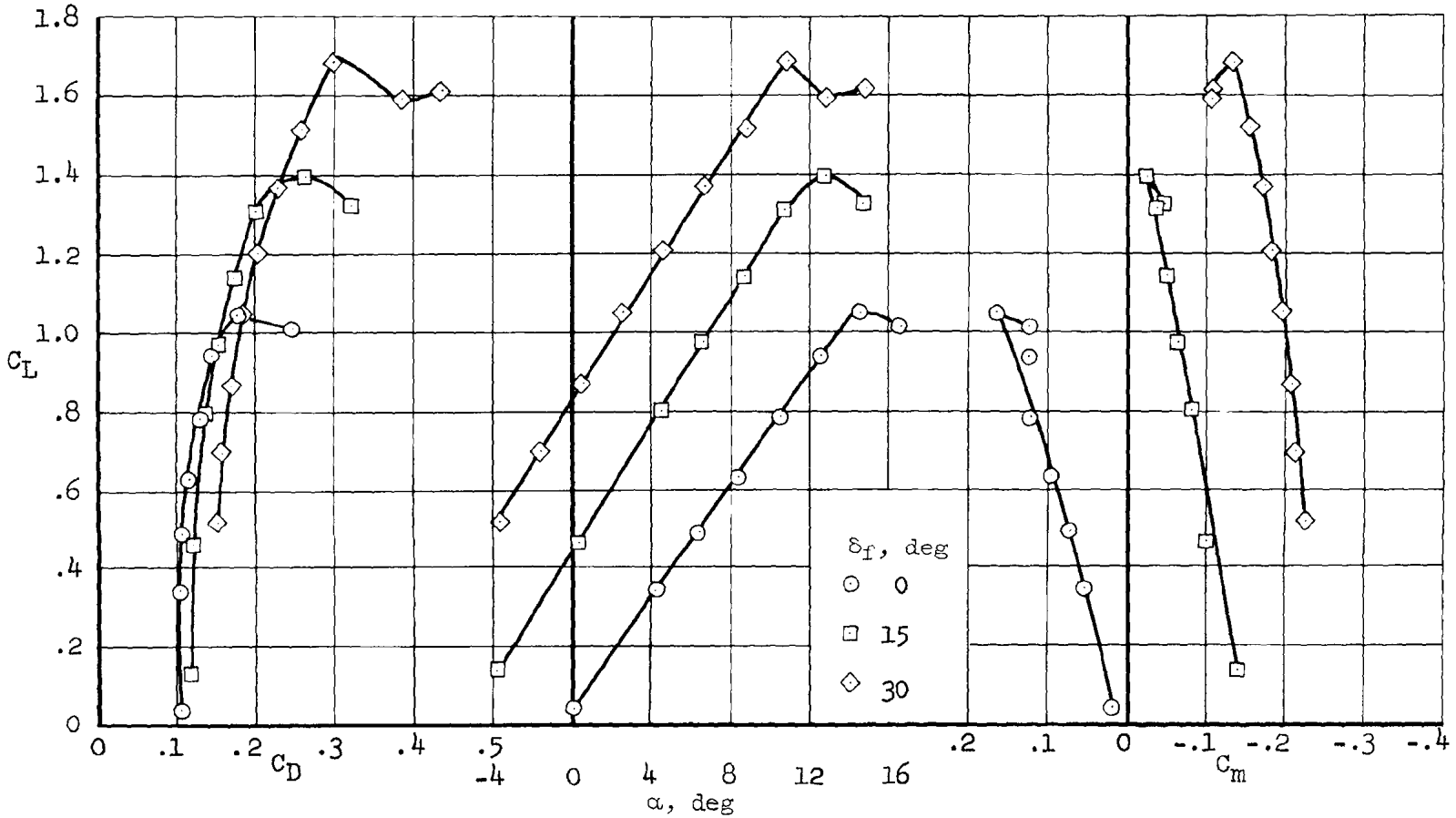

(a) Horizontal tail off.

Figure 20.- Longitudinal characteristics with power off, duct closed, full-span flap; V_∞ = 60 knots.

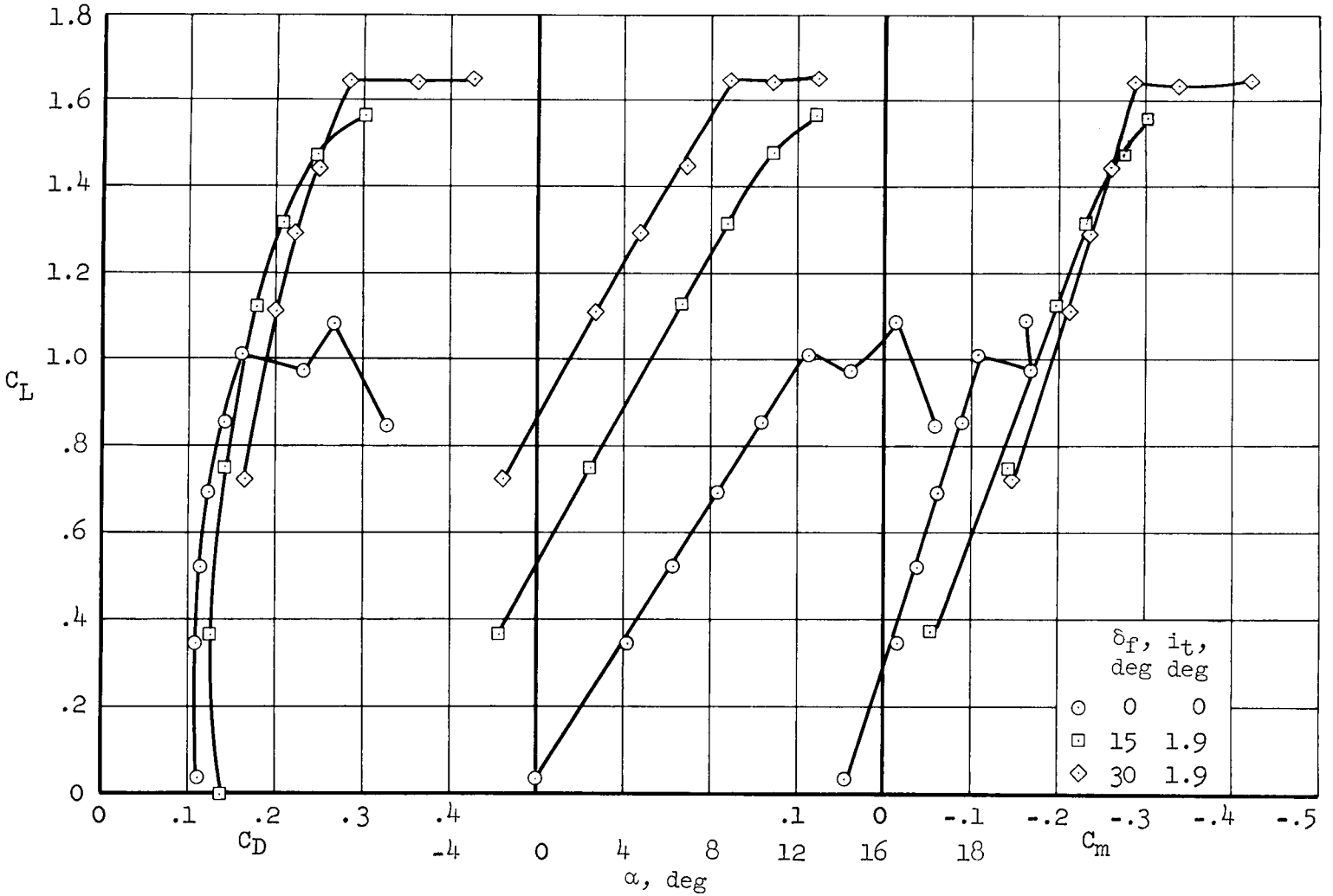

(b) Horizontal tail on, high position.

Figure 20.- Concluded.

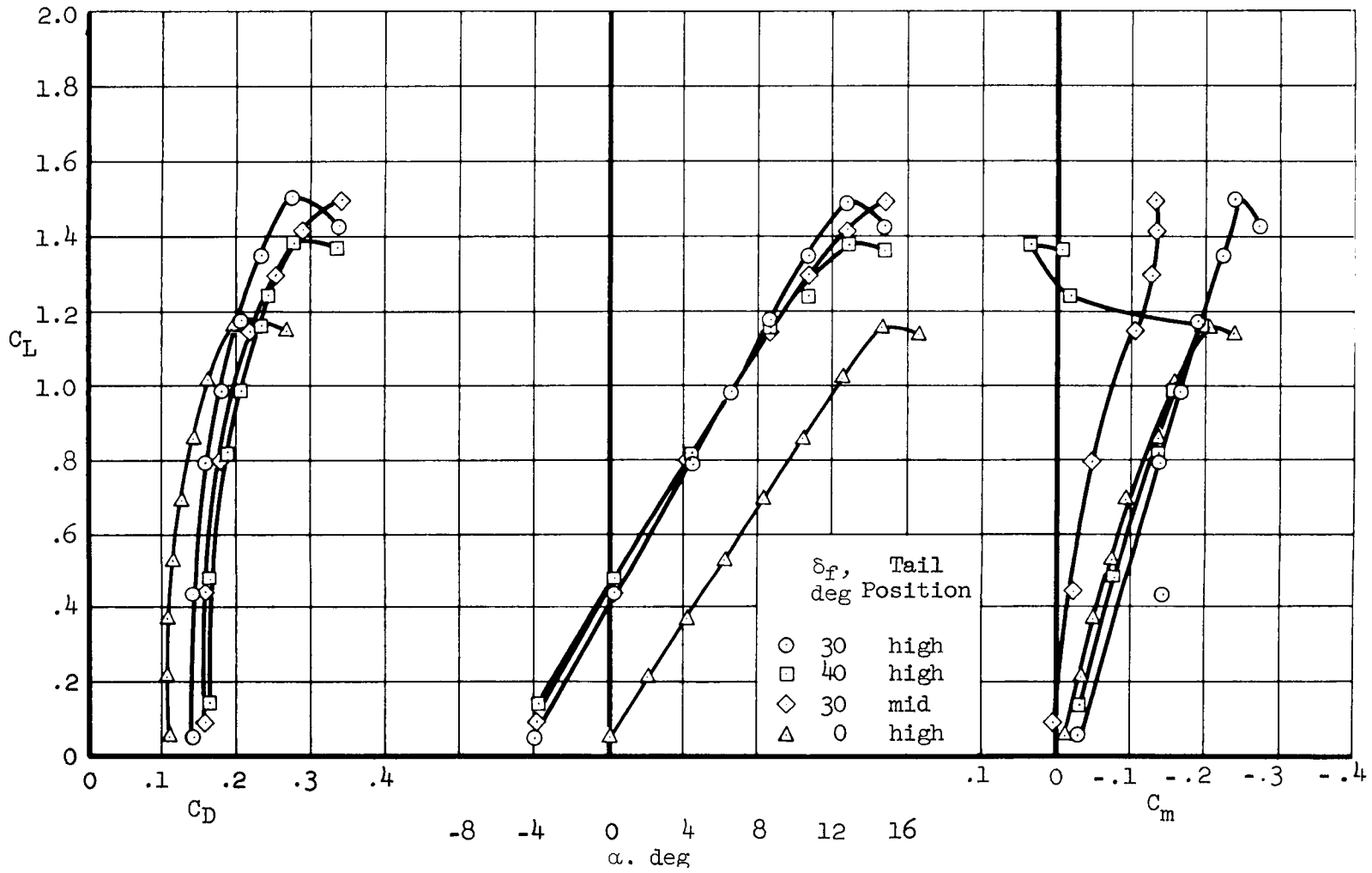

Figure 21.- Effect of tail position and flap deflection on longitudinal characteristics; partial-span flap, fan duct closed, V_∞ = 60 knots, second phase of test.

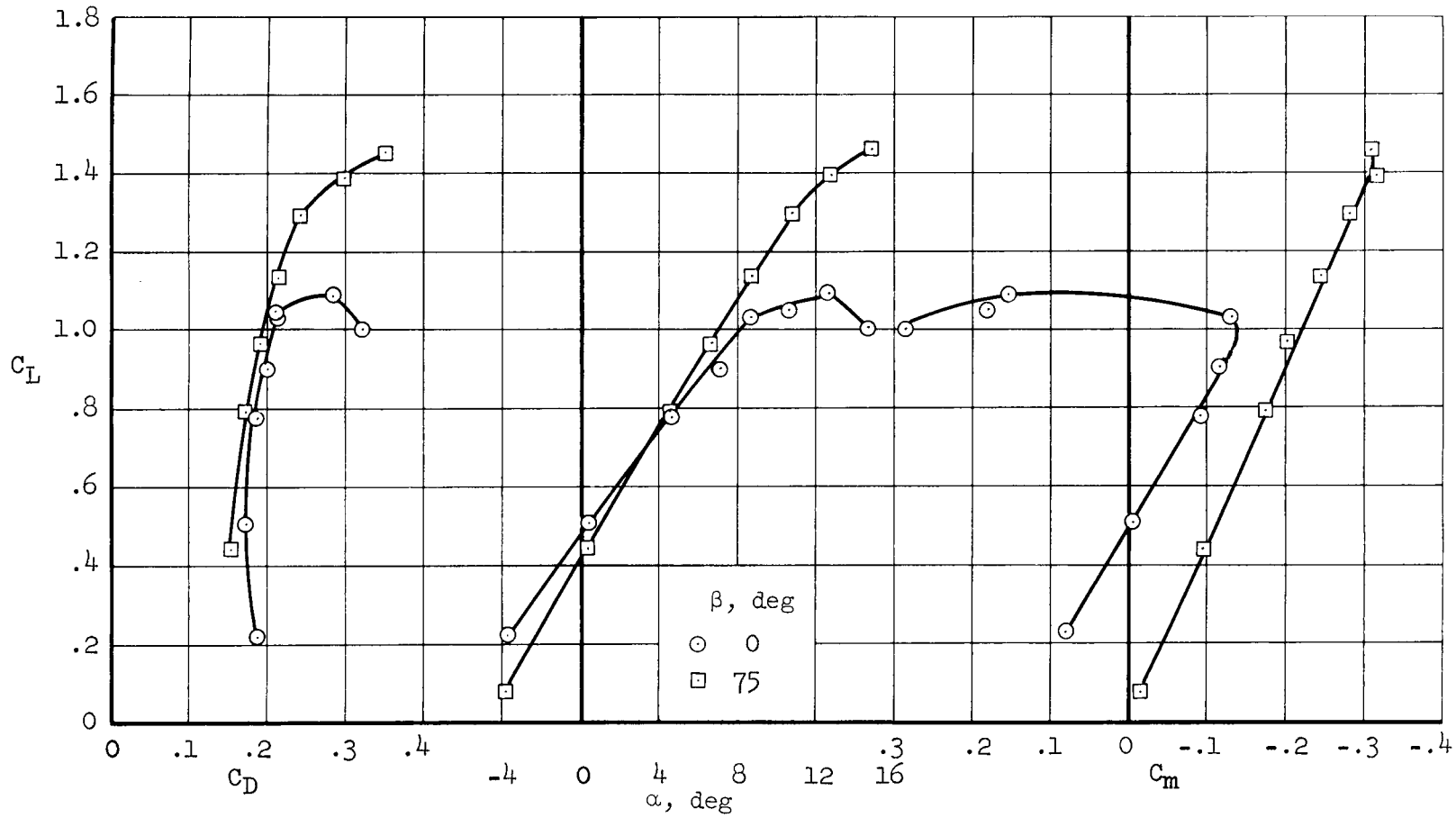

Figure 22.- Longitudinal characteristics with the inlet open and power off; partial-span flap, high tail position, V_∞ = 40 knots, second phase of test, δ_f = 30°.

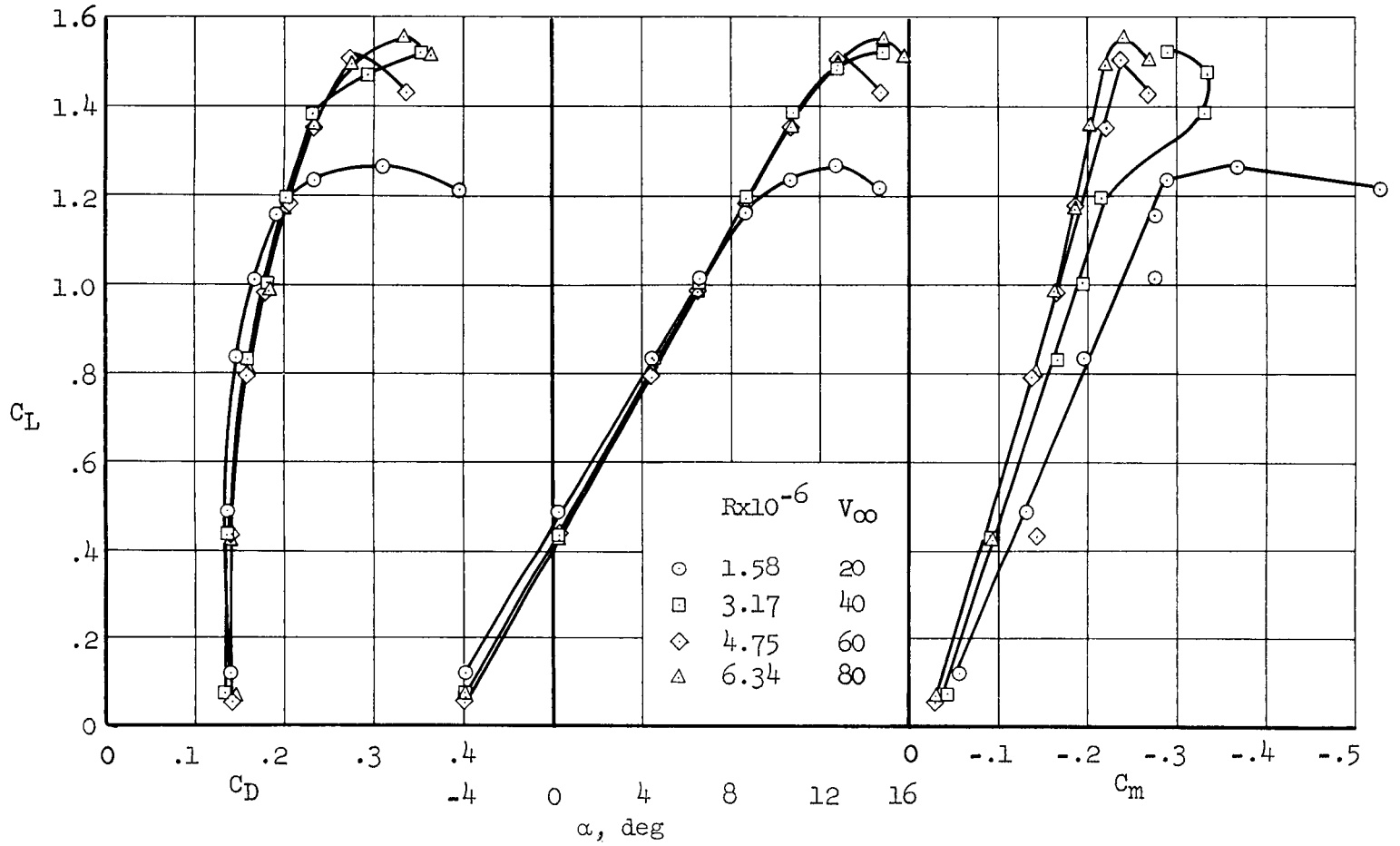

Figure 23.- Effect of Reynolds number on longitudinal characteristics; $\delta_f = 30^\circ$, partial-span, duct closed, high tail position, second phase of test.

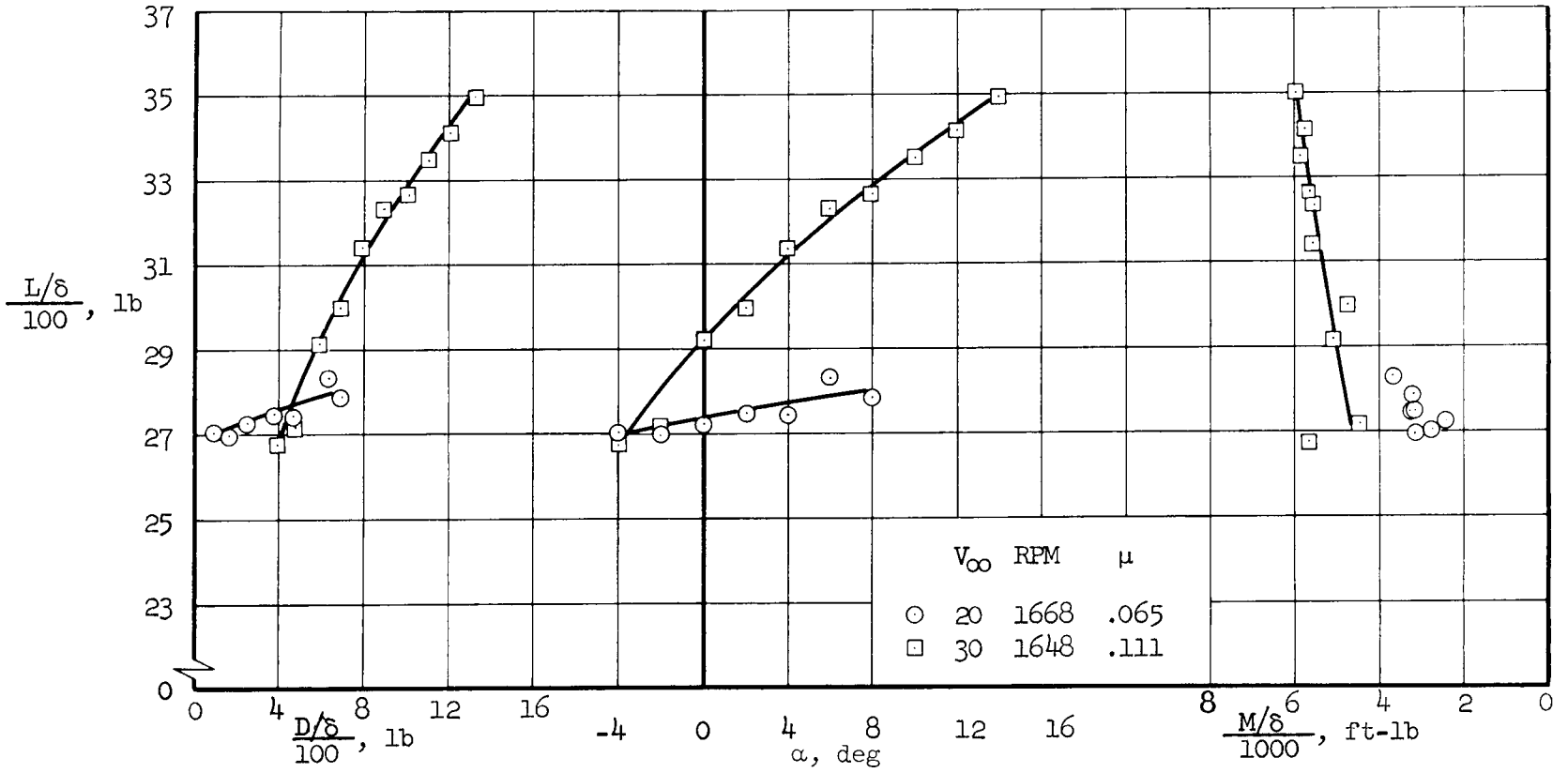

(a) Low-speed forces.

Figure 24.- Longitudinal characteristics with the fan operating, horizontal tail off; $\delta_f = 0^\circ$, $\beta = 0^\circ$, second phase of test.

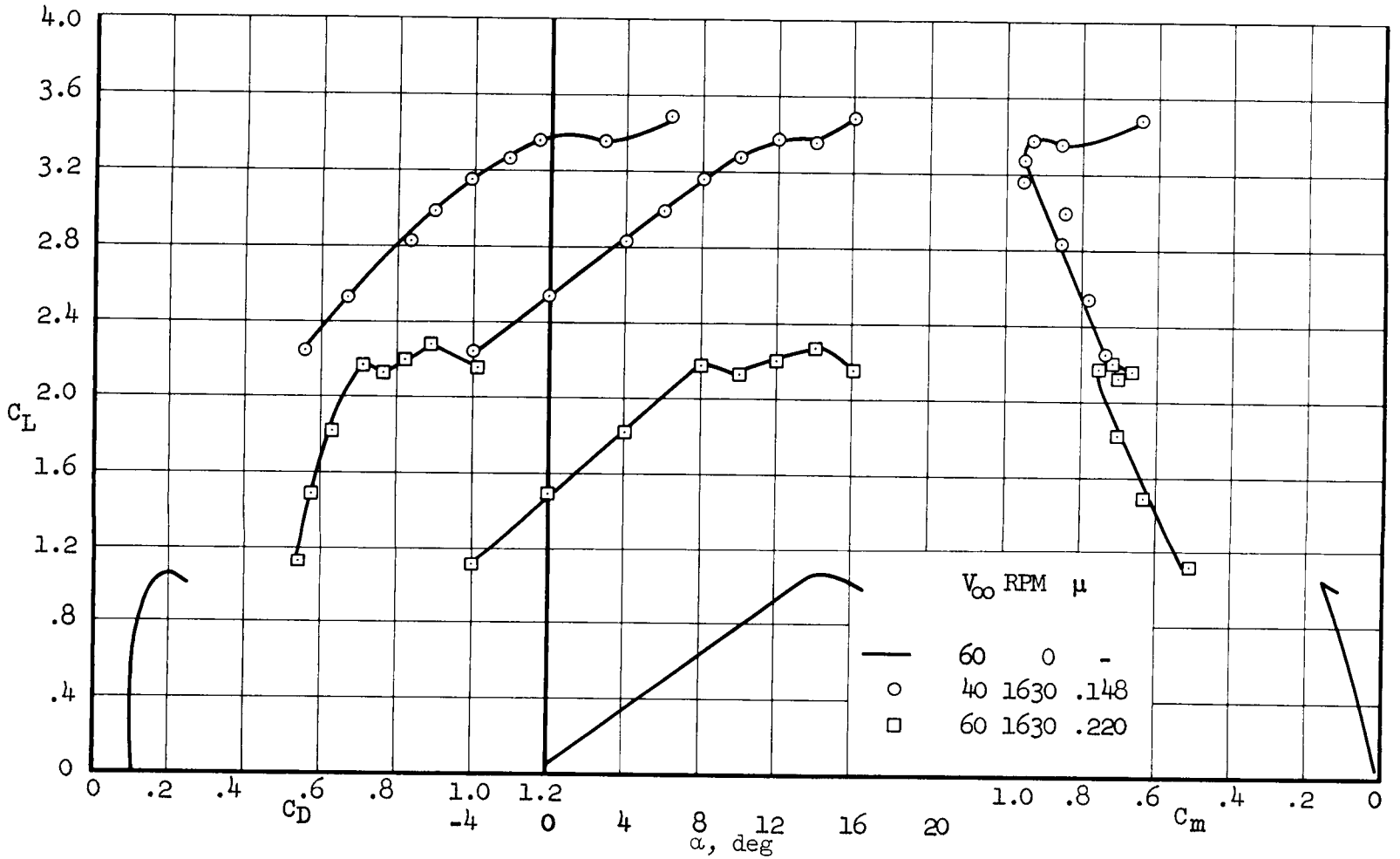

(b) Higher speed coefficients.

Figure 24.- Concluded.

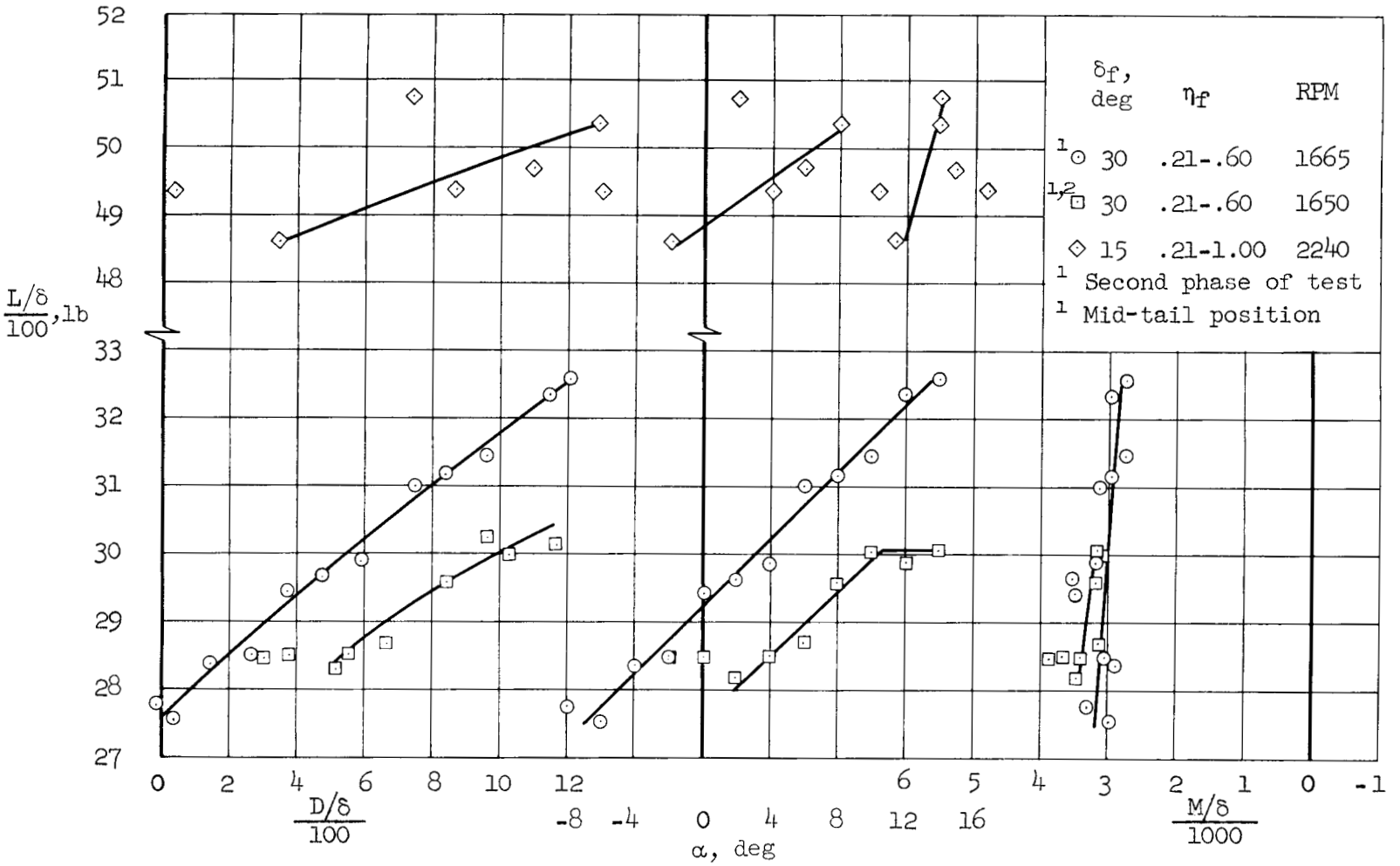

Figure 25.- Power-on longitudinal characteristics; $\beta = 0^{o}$, $V_{\infty} = 20$ knots.

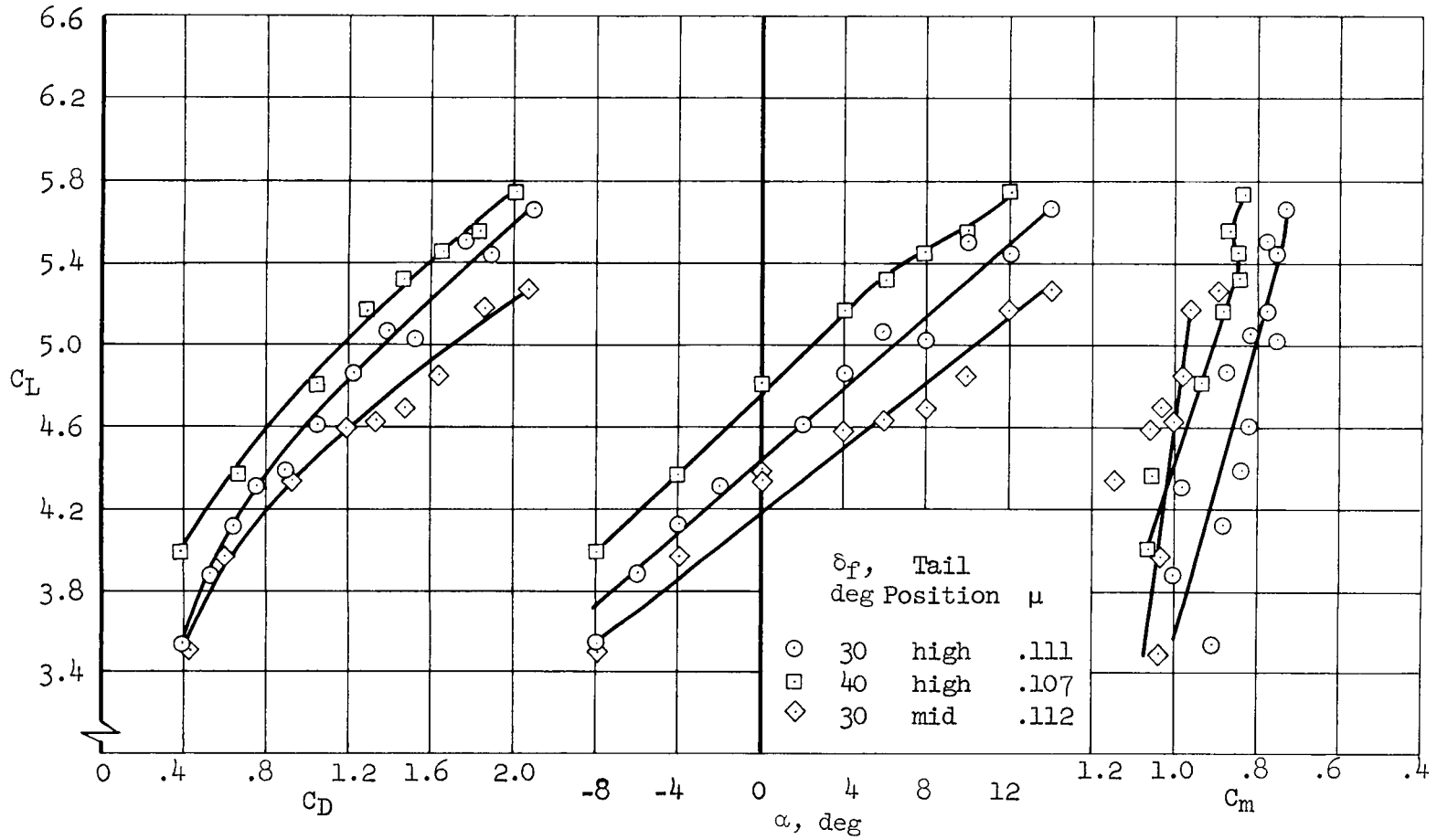

Figure 26.- Power-on longitudinal characteristics with the partial-span flaps and two horizontal-tail heights; $\beta = 0^{\circ}$, $V_{\infty} = 30$ knots, 1650 RPM, second phase of test.

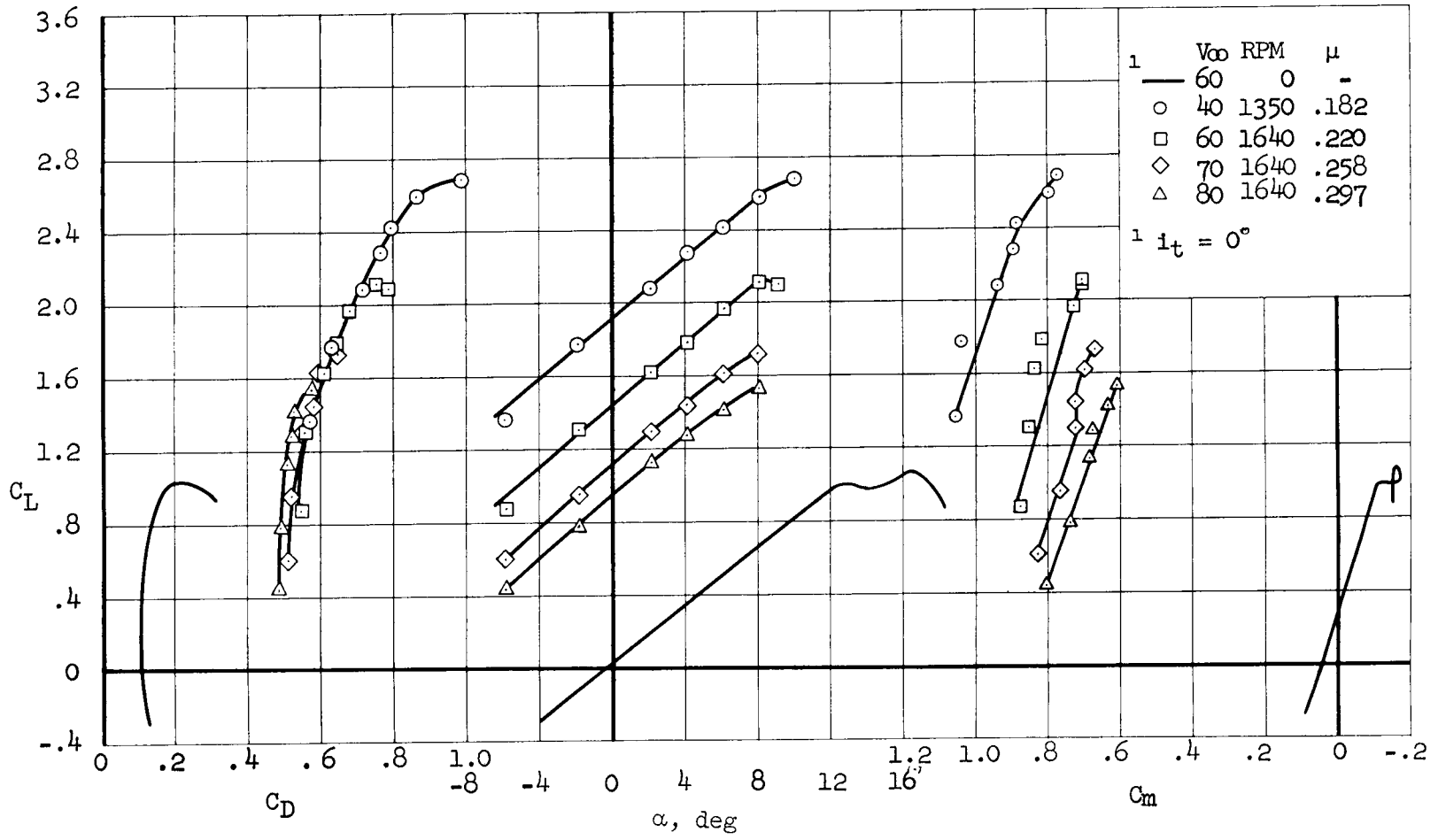

(a) $\delta_f = 0°$, $i_t = -3.7°$

Figure 27.- Power-on longitudinal characteristics; high tail position, full-span flaps, $\beta = 0°$.

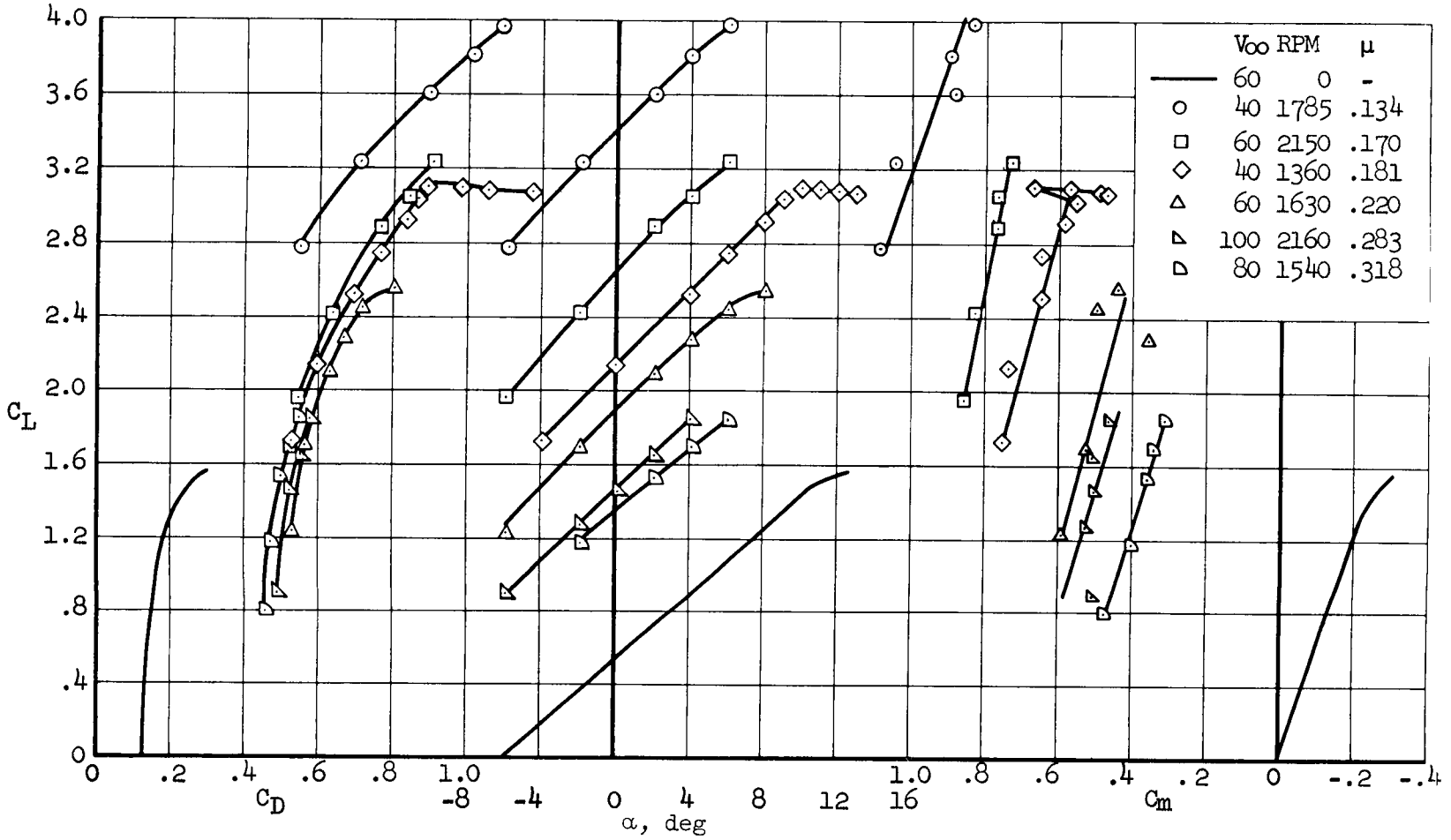

(b) $\delta_f = 15°$, $i_t = 1.9°$

Figure 27.- Continued.

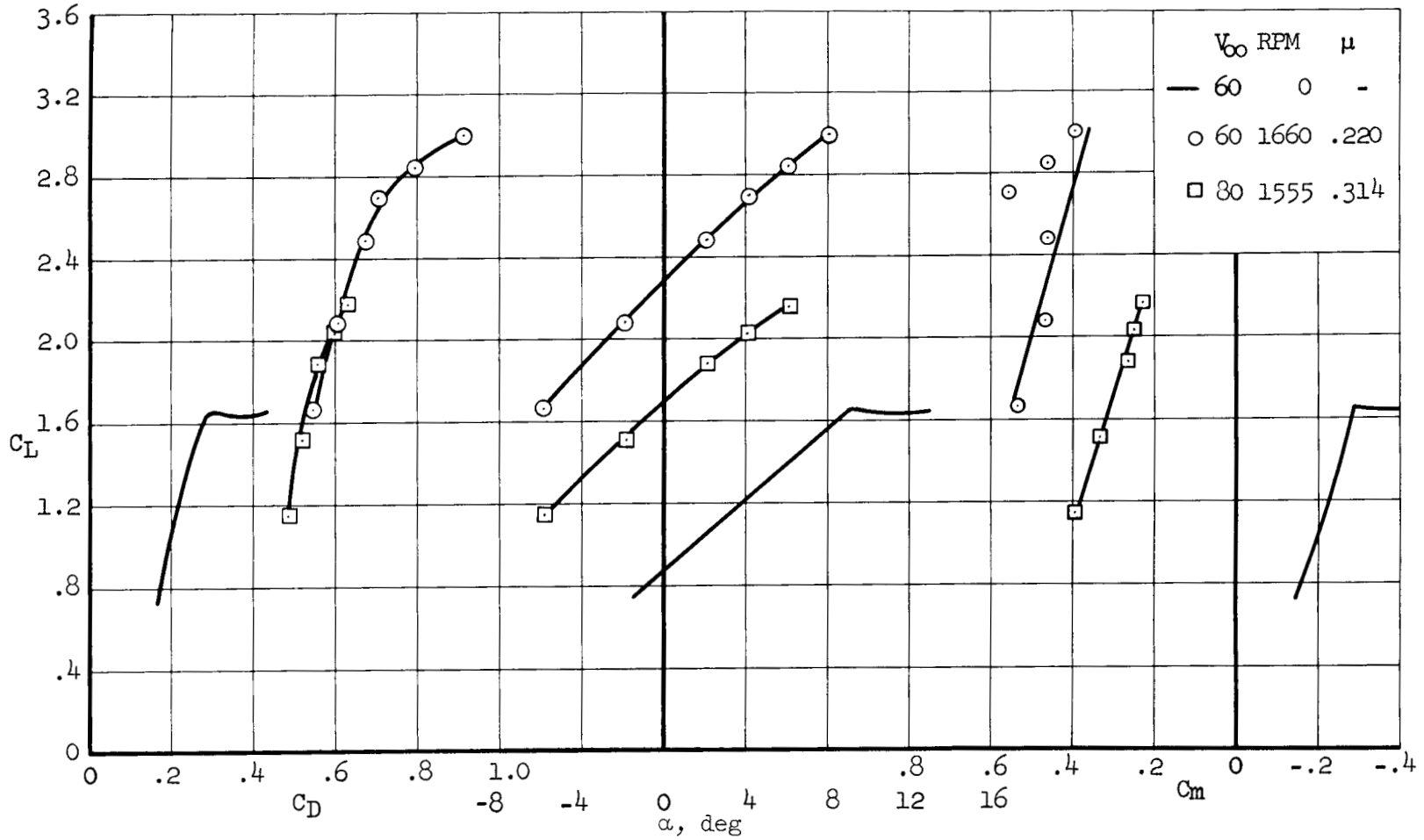

(c) $\delta_f = 30^\circ$, $i_t = 1.9^\circ$

Figure 27.- Concluded.

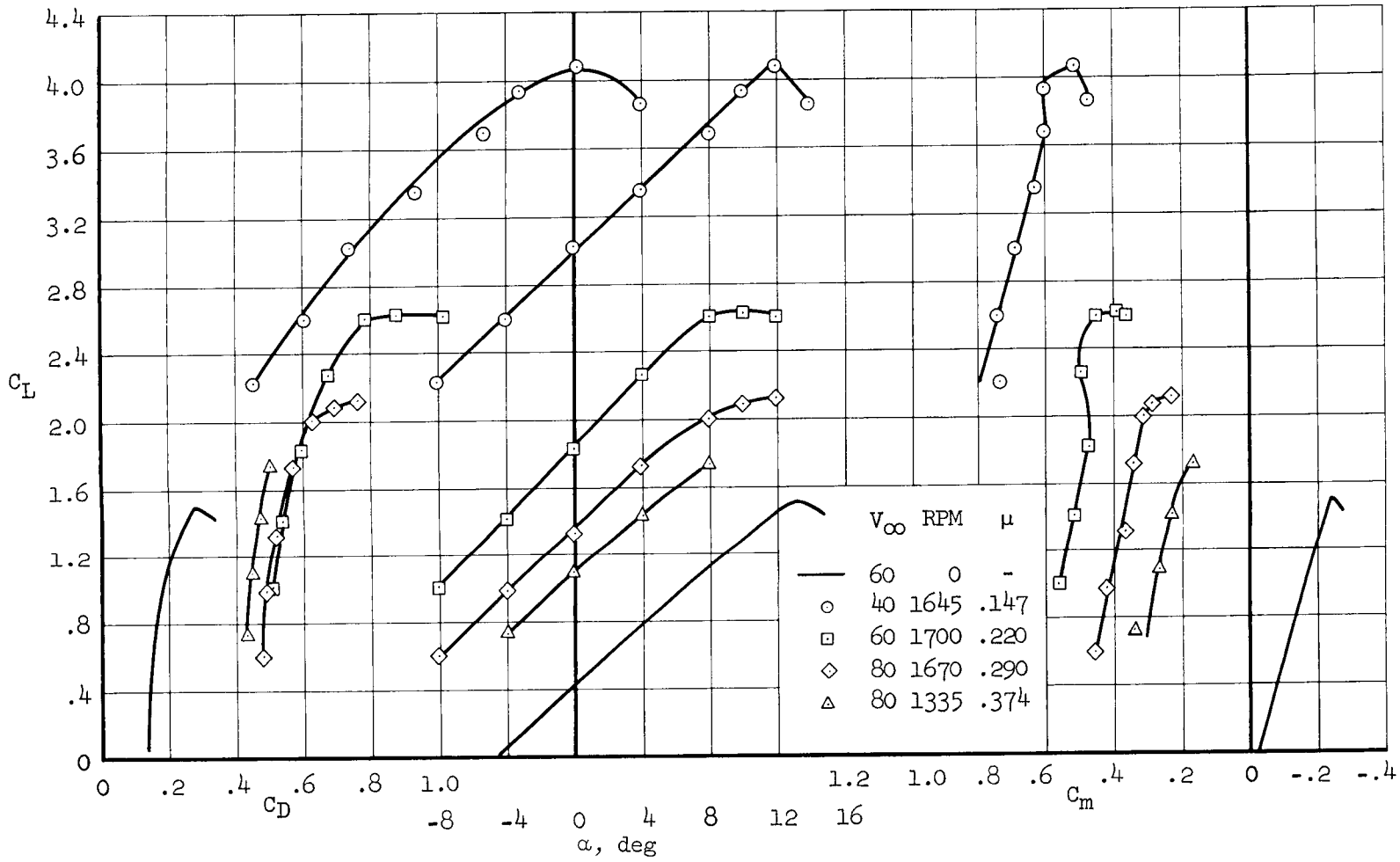

(a) $\delta_f = 30^\circ$, high tail position.

Figure 28.- Power-on longitudinal characteristics with the partial-span flap; $\beta = 0^\circ$, second phase of test.

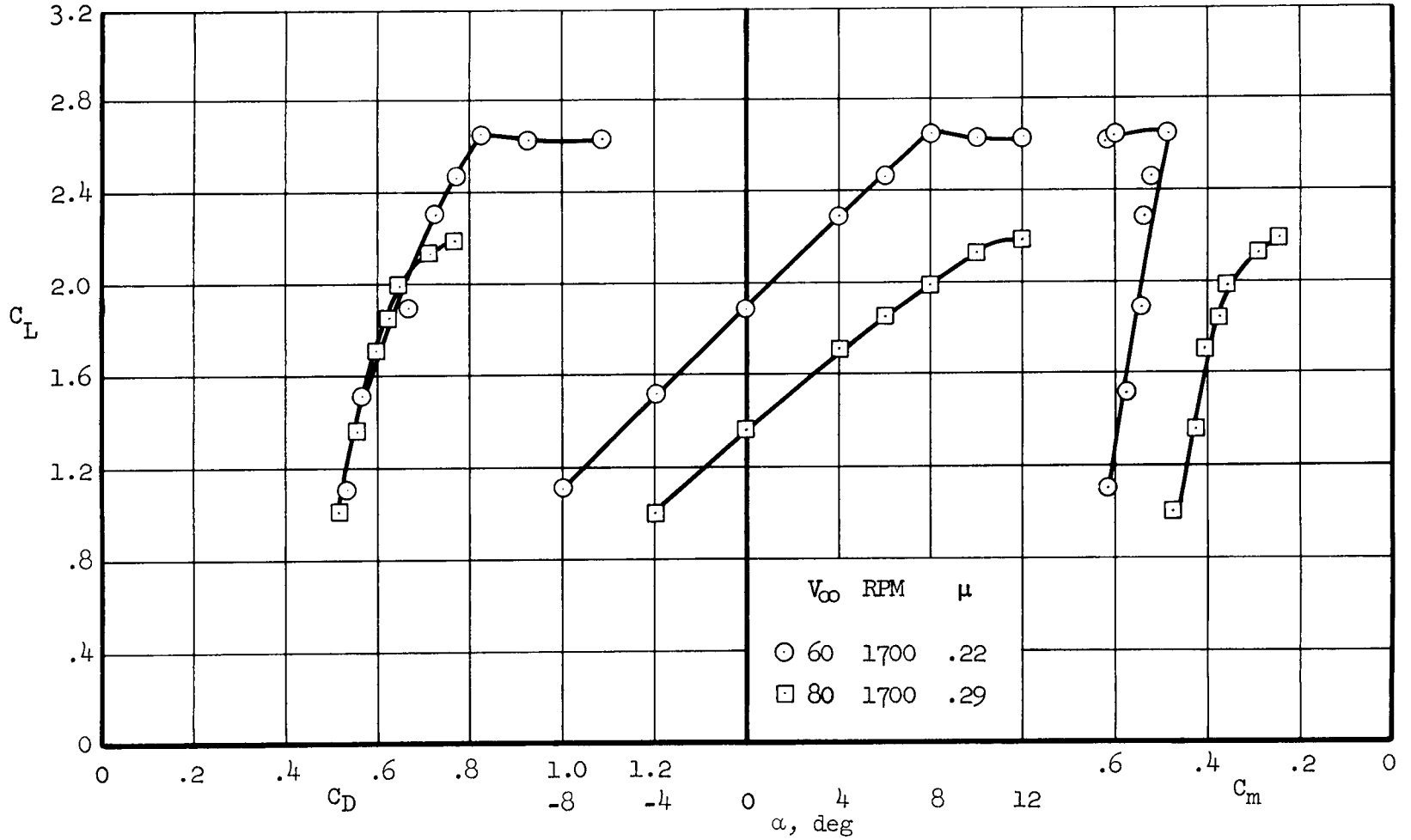

(b) $\delta_f = 40^\circ$, high tail position.

Figure 28.- Continued.

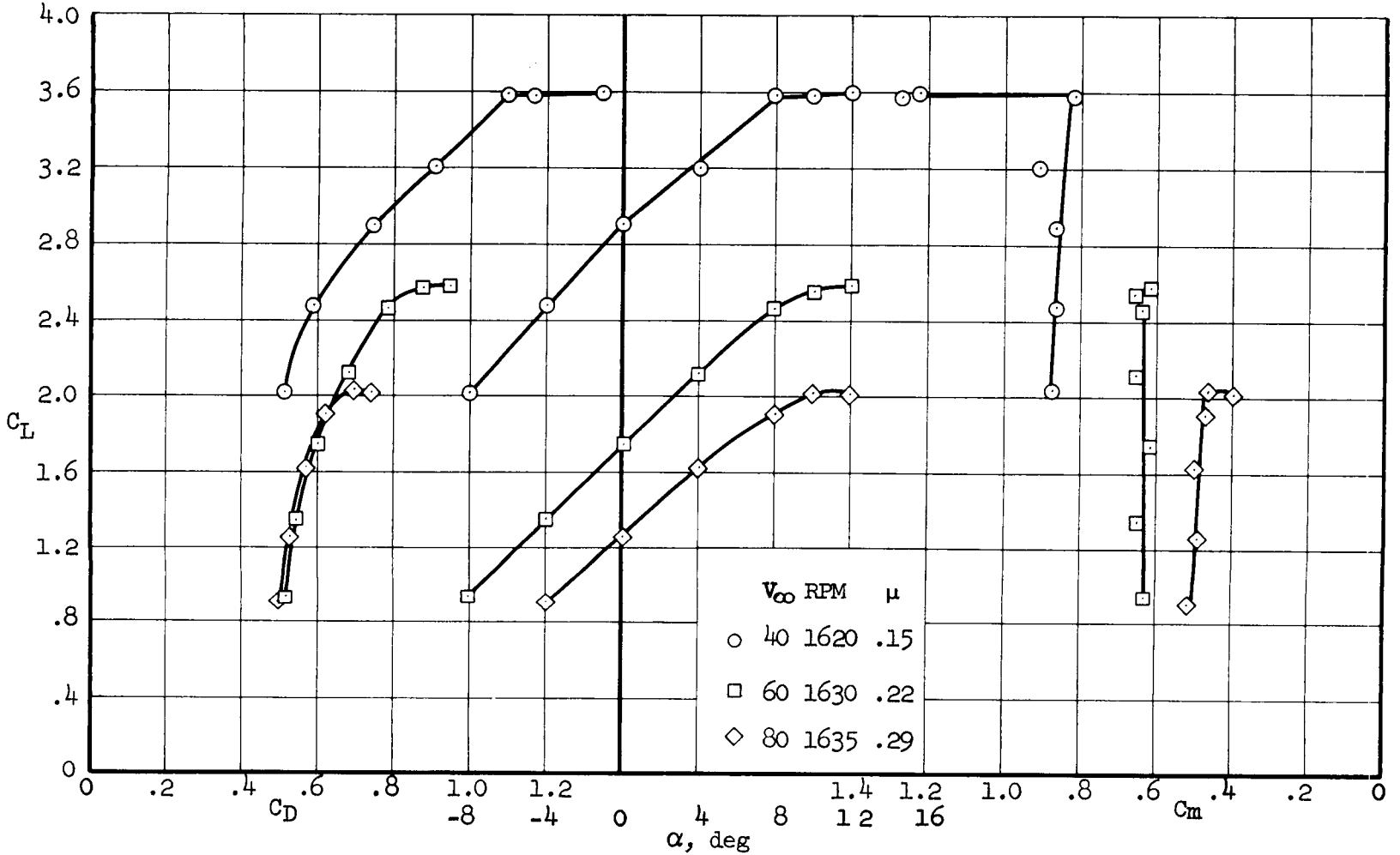

(c) $\delta_f = 30^\circ$, mid tail position.

Figure 28.- Concluded.

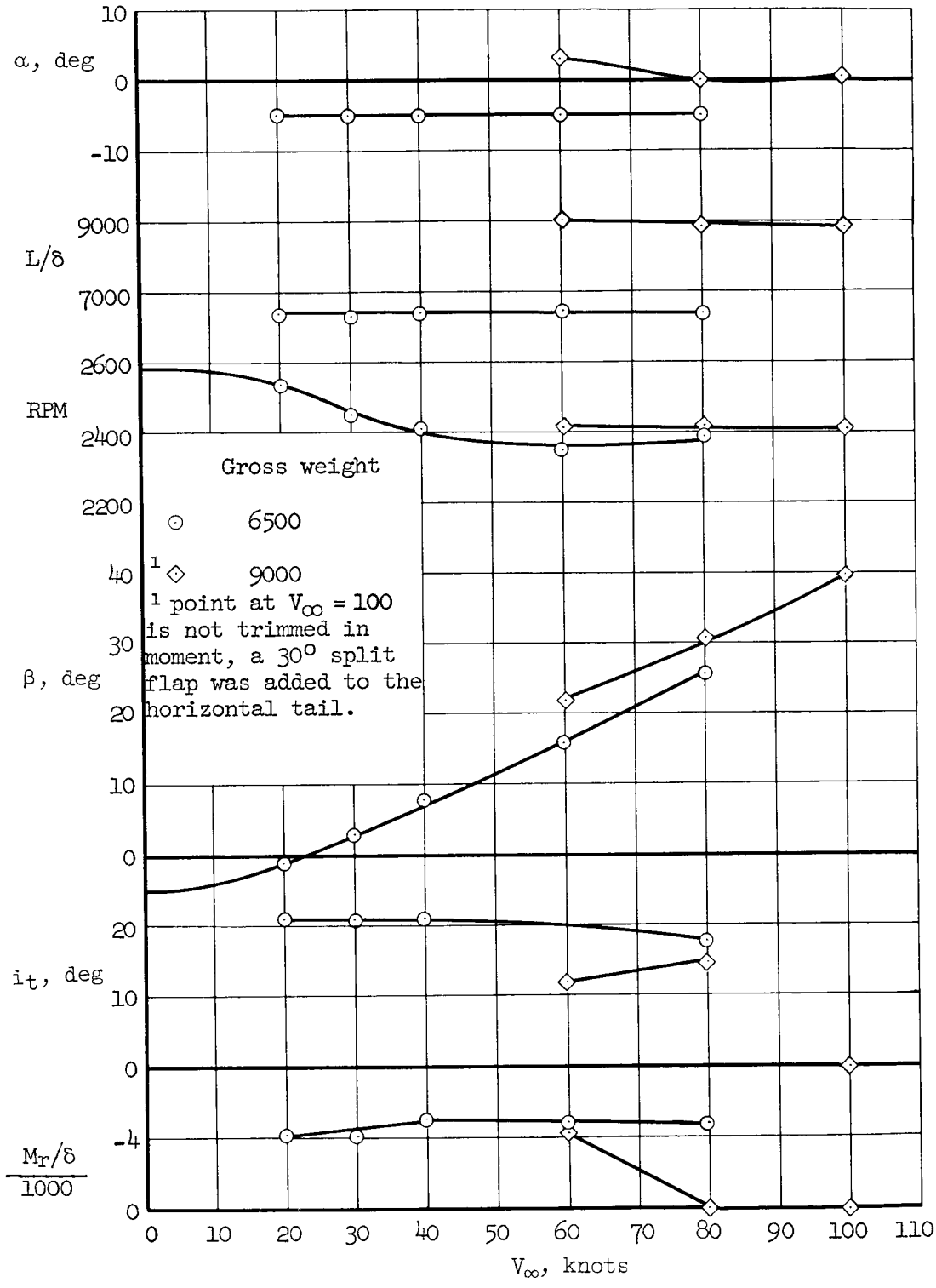

Figure 29.- Measured power and control requirements for zero drag and moment and two values of lifts, partial-span flap deflected 30°, second phase of test.

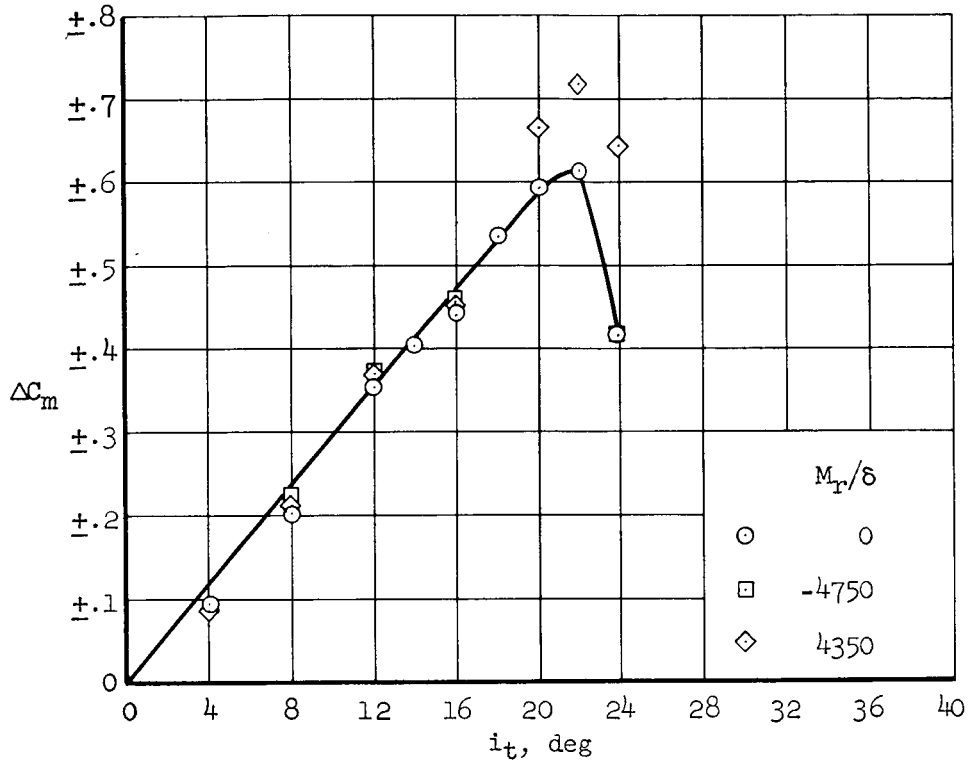

(a) Horizontal-tail effectiveness.

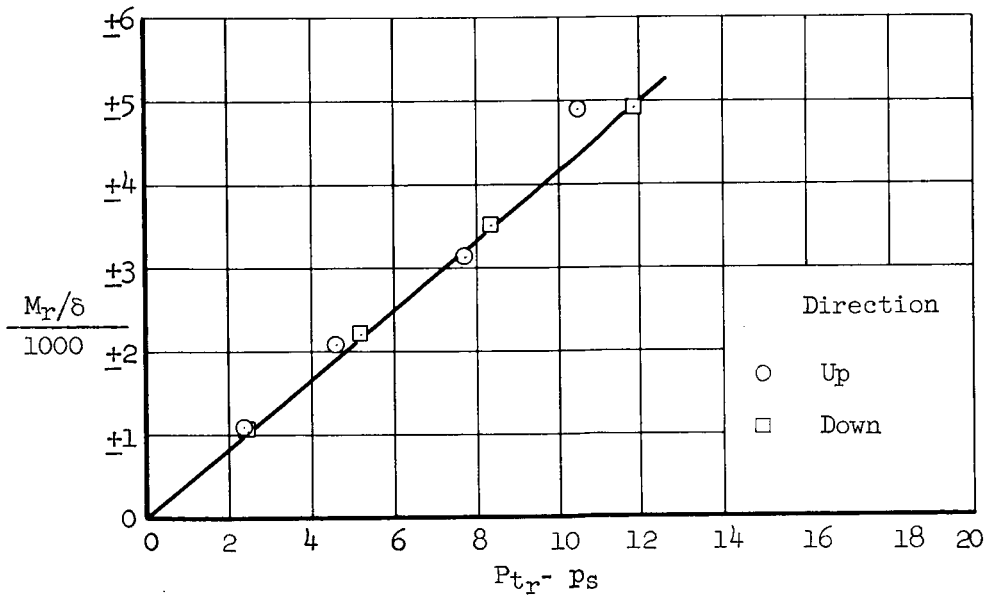

(b) Reaction control power.

Figure 30.- Horizontal-tail and reaction control effectiveness, mid tail position; V_∞ = 40 knots.

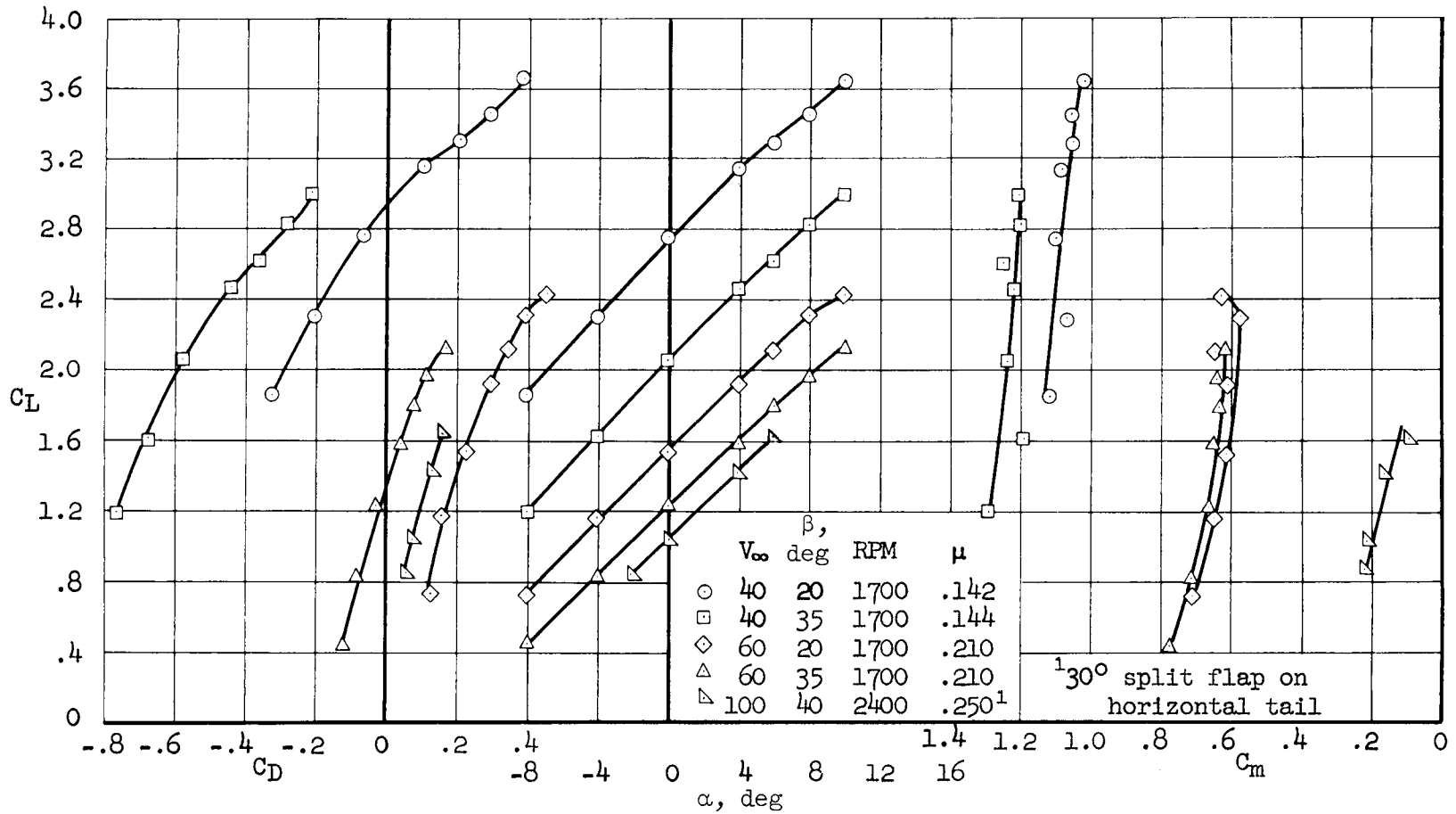

Figure 31.- Power-on longitudinal characteristics with exit vanes adjusted to give near zero drag, partial span flap deflected 30°, high tail position, i_t = 0°, second phase of test.

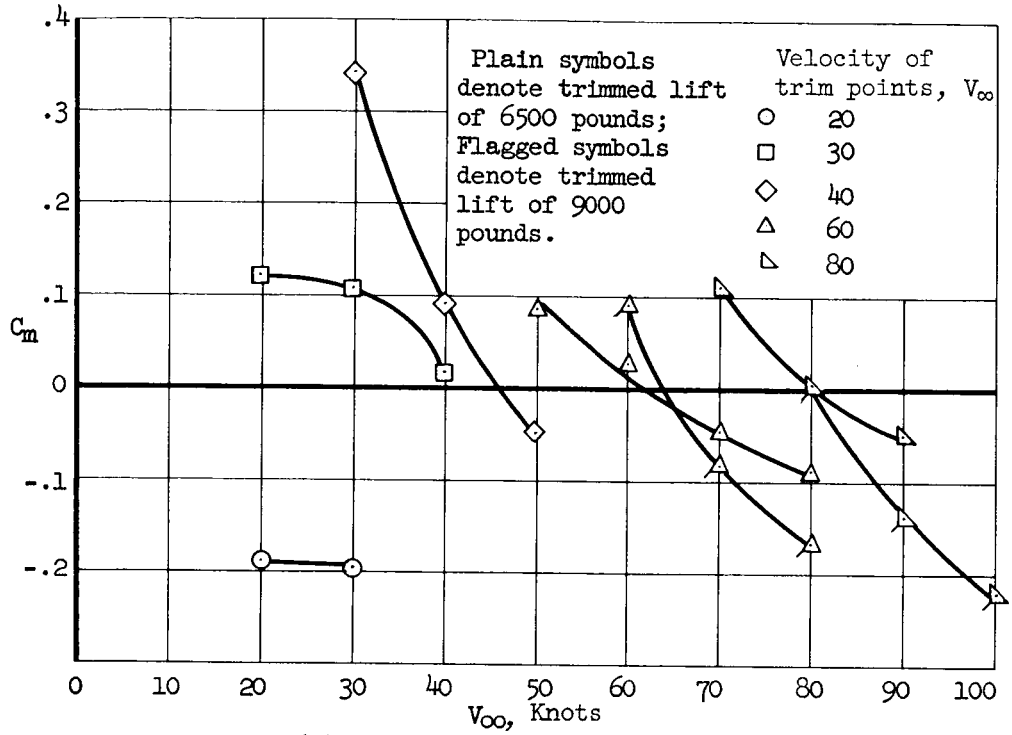

(a) Variation of moment coefficient

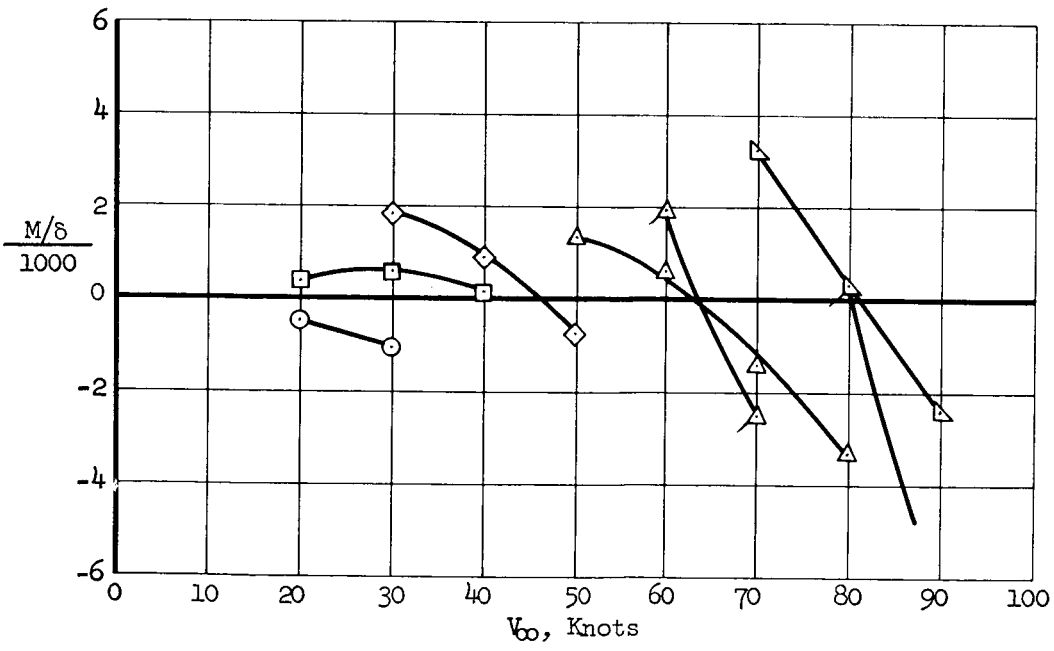

(b) Variation of moment.

Figure 32.- Variation of pitching moment with speed, model near zero drag and moment at trim speed (see fig. 29), partial-span flap deflected 30°, second phase of test.